공학석사 학위논문

해양구조물 체결을 위한 A16061 합금 볼트의 통합 제조공정 설계

Integrated Manufacturing Process Design of Al6061 Alloy Bolts for Fastening Offshore Platforms

지도교수 이 경 훈

2019년 2월

한국해양대학교 대학원
기관공학부

박 성 철

본 논문을 박성철의 공학석사 학위논문으로 인준함

위원장 : 심 도 식 인

위 원 : 이 경 훈 인

위 원 : 김 명 환 인

2018 년 12 월 18 일

한국해양대학교 대학원

목 차

List of Tables

List of Figures

〈국문초록〉

해양구조물 체결을 위한 Al6061 합금 볼트의 통합 제조공정 설계

박 성 철

기관공학부
한국해양대학교 대학원

초록

최근 수송 분야에서 경량화에 대한 관심이 증가하면서, 각종 수송 기계 부품에 비철금속을 적용하는 사례가 늘고 있다. 특히, 6xxx 계열의 알루미늄 합금은 낮은 비중량, 우수한 기계적 특성 및 높은 내식성으로 인해 소형 선박에서부터 해양 구조물에 이르기까지 다양한 해양 분야에 적용되고 있다. 패스너를 사용한 기계식 체결은 사용이 쉽고 적용이 용이하여 알루미늄 합금과 강재의 접합에 널리 사용되어왔다. 현재까지도 산업 현장에서는 알루미늄 합금과 강재의 체결을 위해 스테인리스강 볼트가 사용되고 있다. 그러나 알루미늄 합금의 모재에 기존의 스테인리스강 볼트를 사용하게 되면 중량의 증가뿐만 아니라 알루미늄 모재에서 갈바닉 부식이 발생하게 되고 이것은 특히 해양 환경에서 더욱 가속화된다. 따라서 스테인리스강 볼트를 알루미늄 합금 볼트로 대체하는 것은 추가적인 경량화를 도모할 수 있을 뿐만 아니라 해양 환경에서 이러한 갈바닉 부식의 생성을 미연에 방지할 수 있다.

현재까지 알루미늄 합금 볼트 성형에 대해 일부 연구들이 수행되어 왔다. 그러나 대부분의 연구들은 재료의 성형성 평가에 국한되어 있으므로 성형 공정에 대한 명확하고 체계적인 설계 기준이 없다. 또한, 볼트를 제조하기 위해

필수적인 트리밍 및 전조 공정의 설계가 누락되어있다.

따라서 본 연구에서는 해양구조물 체결을 위한 Al6061 합금 볼트의 통합 제조공정 설계를 수행하였다. 이를 위해 이론 설계 및 수치 해석을 진행하였다. 이론 설계에서는, 스크류 규격과 기하학적 관계를 고려하여 전조 공정의 초기 소재경과 압입 깊이를 계산하였다. 헤딩 공정을 위한 초기 소재 치수는 체적일정법칙으로 구하였다. 결함 예측에 사용되는 공정 한계를 고려하여, 공정 단수를 설정하고, 헤딩 공정의 설계 규칙에 의해 예비 형상을 결정하였다. 또한 설계된 헤딩 공정에 대해 슬래브법을 사용하여 성형 하중을 예측하였다. 이론 설계를 바탕으로 헤딩, 트리밍 및 전조 공정에 대한 유한요소해석을 수행하였다. 헤딩 및 트리밍 공정 중에 발생하는 결함을 예측하기 위해 연성파괴기준을 적용하였다. 또한 전조 공정에서 금형의 압입량, 이송 속도 및 분당 회전수, 트리밍 공정에서는 펀치의 곡률 반경, 하부 금형의 랜드 폭 및 펀치와 하부 금형간의 정지 거리를 각각 설계 변수로 선정하고 다구찌법을 통해 공정을 최적화하였다. 제안 된 설계 방법을 검증하기 위해 알루미늄 합금 볼트 성형 실험을 수행하였고 높은 치수 정확도를 갖는 건전한 형상의 Al6061 합금 볼트를 얻을 수 있었다.

KEY WORDS: 알루미늄 합금 볼트; 통합 제조공정 설계; 유한요소해석; 연성파괴기준; 다구찌법.

<영문초록>

Integrated Manufacturing Process Design of Al6061 Alloy Bolts for Fastening Offshore Platforms

Park, Sung Cheol

Division of Marine Engineering
Graduate School of Korea Maritime and Ocean University

Abstract

In recent years, with the increasing interest in weight reduction in the transportation sector, the application of non-ferrous metals to various transportation machinery parts has been increased. In particular, the 6xxx series of aluminum alloys are commonly used in marine applications from small vessels to offshore structures due to its low specific weight, high quality mechanical properties, and high resistance to corrosion. In order to join aluminum alloy and steel, mechanical joint by fasteners has been widely used because it is easy-and-practical for the application. Until now, stainless steels bolts have been used for fastening aluminum alloys and steels to industrial sites. However, when the stainless steel bolt is used for the base material of aluminum alloy, weight increases and galvanic corrosion occurs in aluminum, which is accelerated in marine environment particularly. Therefore, substituting aluminum alloy bolts for stainless steel ones can prevent such corrosion promotion in marine environment as well as extra weight increase.

To date, several studies have been conducted on aluminum alloy bolt forming. However, most studies are limited to the evaluation of formability of materials, so there is no clear and systematic design criterion for the forming process. Furthermore, the design of the trimming and thread-rolling process, essential for manufacturing bolts, was not considered.

Therefore, the integrated manufacturing process design of Al6061 alloy bolts for fastening offshore platforms was performed in this study. To do this, we carried out theoretical design and numerical analysis. At theoretical design, the initial rod diameter and the penetration depth in thread-rolling process were calculated according to the screw standards and geometric relation. Thereafter, the dimensions of the initial workpiece for the heading process were obtained by volume constancy law. Considering process limitations to predict the defects, the number of the stage was set, and preform was determined by the design rule in the heading process. In addition, the forming load for the designed heading process was predicted by using the slab method. Based on theoretical design, FE-analysis for the heading, trimming and thread-rolling process was conducted. The ductile fracture criterion was applied to predict the defects during the heading and trimming process. In addition, the Taguchi method is used to optimize the trimming and thread-rolling process with the set of design parameters, such as the penetration depth, transfer velocity, and revolutions per minute of rolling dies in the thread-rolling process, and the blade radius of the punch, land width of the bottom die, and stop distance between the punch and bottom die in the trimming process, respectively. To verify the proposed design, the aluminum alloy bolt forming experiment was carried out and sound Al6061 alloy bolt with high dimensional accuracy was obtained.

KEY WORDS: Aluminum alloy bolts; Design of integrated manufacturing process; FE-analysis; Ductile fracture criterion; Taguchi method.

1. Introduction

1.1 Research background

Based on rising economic and political demand to reduce fuel consumption and CO_2 emissions of transportation machinery such as automotive, aircraft and ship, the efforts to reduce the weight of various mechanical parts in the transportation industry have increased significantly, and the application of non-ferrous metal with high strength to weight is increasing. In this trend, aluminum alloys are in the spotlight due to their excellent mechanical characteristics such as good machinability, weldability, high fatigue strength and good corrosion resistance in seawater environments. In particular, the usage of aluminum alloys for the marine industries varies from merchant ships to offshore plants, warships and leisure vessels[1-3]. Fig. 1 shows an aluminum alloy helideck on offshore platforms.

In general, when the base metal is an aluminum alloy, stainless steel is mainly used as the material of the fasteners. In this case, depending on the material of the fasteners (Steel, Cast Iron, SUS304 / 316), galvanic action causes a defect that the base material is corroded. According to AISI 502-476-18M-CP, "Stainless Steel Fasteners: A Systematic Approach To Their Selection" (See Table 1), the corrosion of the base material is promoted in the above case and this effect is accelerated in marine environment particularly. In addition, using stainless steel bolts cause the increase of the total weight of machinery. It was found that replacing the fastening material with the same kind of aluminum alloy reduces the corrosion of the base material. Therefore, when aluminum alloy bolts are used for aluminum alloy components, such corrosion promotion in marine environment can be prevented and the extra weight reduction can be attained as well.

Fig. 1 Aluminum alloy helideck on offshore platforms

Table 1 Guideline for selection of fasteners based on galvanic action

Base Metal	Fastener Metal					
	Zinc & Galvanized steel	Aluminum & Aluminum Alloys	Steel & Cast Iron	Brass, Cooper, Bronze, Monel	Martensitic Stainless (Type 410)	Austenitic Stainless (Type 304, 316, etc.)
Zinc & Galvanized steel	A	B	B	C	C	C
Aluminum & Aluminum Alloys	A	A	B	C	Never recommended	B
Steel & Cast Iron	AD	A	A	C	C	B
Lead-Tin Plated sheets	ADE	AE	AE	C	C	B
Brass, Copper, Bronze, Monel	ADE	AE	AE	A	A	B
Ferritic Stainless (Type 430)	ADE	AE	AE	A	A	A
Austentic Stainless (Type 304 316, etc.)	ADE	AE	AE	AE	A	A

A-The corrosion of the base metal is not increased by the fastener.
B-The corrosion of the base metal is marginally increased by the fastener.
C-The corrosion of the base metal may be markedly increased by the fastener material.
D-The plating on the fastener is rapidly consumed, leaving the bare fastener metal.
E-The corrosion of the fastener is increased by the base metal.
NOTE: Surface treatment and environment can change activity.

1.2 Precedent research

To date, several studies have been conducted on aluminum alloy bolt forming. Shin and Kawai (1991) performed die geometry optimization for the multi-stage cold forging process using Al1100 alloy. The effects of the radius of the corner of the lower die and the angle of the upper die for preforming on the forging load and final product shape were investigated[4]. Yoon, et al. (2012) investigated the effects of homogenization annealing and age hardening on Al-Zn-Mg-Sc alloy bolt forming, and predicted the growth of defects using finite element (FE) analysis[5]. Kim, et al. (2010) proposed a suitable preform for Al-Zn-Mg alloy bolt forming by applying the ductile fracture theory to predict the internal defects of the products. In addition, the internal crystal changes caused by the aluminum alloy heat treatment were analyzed[6]. Im, et al. (2010, 2012a, b) conducted research on the development of high-strength aluminum alloy bolts through grain refinement by applying the equal channel angular process (ECAP), which is a severe plastic deformation (SPD) method. Aluminum alloy bolts manufactured by ECAP showed better mechanical properties, such as maximum tensile strength, Vickers micro-hardness, and elongation, compared with bolts formed by the conventional process[7-9].

However, these studies focused mainly on the evaluation of the formability and mechanical properties of materials, so there is no clear and systematic design criterion for the formation process of aluminum alloy bolts. Furthermore, the bolt manufacturing process is generally composed of a series of processes, including heading, trimming, and thread-rolling; if needed, heat treatment is included as well. Therefore, it is necessary to develop a specific design method for manufacturing aluminum alloy bolts, considering the entire manufacturing process: heading, trimming and thread-rolling process.

The trimming process refers to a shearing process that removes

unnecessary parts of forged products to create a final product with sound shapes and applied to manufacturing various industrial parts such as bulk and sheet metal products. In the trimming process, if the dimensional accuracy of the shear surface is poor or excessive burrs occur, a post-process is required to correct these forming defects, which causes a decrease in price competitiveness due to an increase in the production cycle. Therefore, it is very important to ensure sound quality of the sheared plane in the trimming process.

So far, trimming process has been studied both experimentally and numerically. Choi, et al. (2012) investigated the effect of clearance and inclined die angle on trimming quality of ultra-high strength steel plate[10]. Lee, et al. (2016) studied the effect of the clearance, blade radius of punch and die, and blade holding force in the trimming process of the automotive door latch on the roll-over and the effective shear surface. Then the optimum trimming process conditions were derived using the Taguchi method[11]. Li (2000) experimentally evaluated the effects of shear angle, punch curvature radius and clearance on shear surface quality and burr height in the trimming process of aluminum plate, and found that a quality cross section was obtained within the specific range of shear angle regardless of the clearance and punch radius[12]. Han, et al. (2016) performed FE-analysis applying ductile fracture models to the trimming process of ultra-high strength hot stamping parts and compared them with experimental results. Also, the effect of clearance, shear angle, and radius of curvature of the punch on the cross sectional shape was investigated[13]. MacCormack and Monaghan (2001a, b) used FE-analysis to optimize the shape of the bolt trimming punch considering tool life. Further, the effect of stop distance between punch and die on shear load by knockout pin and shear quality was investigated[14,15]. Cho, et al. (2008, 2016a, b) proposed a die design method to improve shape

defects during trimming process of flange bolts. In addition, the design of multi-stage cold forging process was carried out to minimize the amount of chips generated in the production of non-axisymmetric cam bolts and to improve the productivity[16-18]. Park and Lee (2018) designed the trimming process by performing FE-analysis based on the mechanical properties and the critical damage value obtained from the tensile test of the material. To do this, the blade radius of the punch, the land width of the bottom die, and the stop distance between the punch and the bottom die were chosen as design parameters, and the process optimization for the shear quality and shear load was performed using the Taguchi method[19].

The thread-rolling process is a processing method in which the material is positioned between the driving and the stationary dies and the threads are fabricated by progressive forming by rotation and indentation of the driving die. The thread-rolling process is generally applied to the manufacture of fasteners such as bolts and screws. Thread rolled screws have the advantage of better surface quality and higher mechanical strength compared with machined products and suitable for mass production[20]. Rotational forming processes, such as thread-rolling, belong to relatively complex computational problems, and numerical methods such as finite element method are mainly used to analyze the process.

Lee, et al. (2016, 2017) examined the forming characteristics of the micro-thread with respect to the height of the thread chamfer and the distance between the dies in flat thread-rolling and further analyzed the thread-rolling process of the asymmetric thread screw to increase the clamping force[21,22]. Domblesky and Feng (2002a, b) performed FE-analysis for the thread-rolling process using a two-dimensional model assuming plane strain, and also performed three-dimensional forming analysis for the flat thread-rolling process. The effects of process parameters such as friction

constant, work hardening coefficient, thread shape, and blank diameter on the effective strain of thread were analyzed[23,24]. Hsia, et al. (2015) compared the analytical results of loads, ditribution of stress and strain, and defects according to the number of elements in the FE-analysis and determined the optimal number of elements considering the accuracy and time of analysis[25]. Kim, et al. (2002) studied the forming characteristics according to the tooth shape, frank angle, friction coefficient, and work hardening coefficient, and presented the formula for selecting the optimal blank diameter in the spindle thread-rolling process[26,27]. Song, et al. (2011, 2012) designed an analytical model for manufacturing micro screw and investigated the effects of friction coefficient, lead angle, effective diameter, and the distance between flat dies on the process[28,29]. Shin, et al. (2009) selected the optimal number of teeth and number of elements for the analytical model considering the calculation time, and studied the effects of process variables such as frank angle, tooth profile, and forming temperature on the forming load and formability[30]. Kramer and Groche (2018) investigated the correlation between process variables such as the lubricating and surface condition, stroke speed and yield strength of material, and defect occurrence during the flat die thread-rolling process. To do this, they developed a sensor system for load measurement, and analyzed the load variation tendency according to the process variables. Investigations have shown that the lubrication between the material and the die affects the increase in the relative slip rate, which is responsible for the increase in load and the occurrence of defects[31]. Park, et al. (2018) has proposed the method to design the thread-rolling process using the FE-analysis and the Taguchi method. To realize the practical design technique, process variables such as penetration depth, transfer velocity and revolution per minute were considered to design and optimize the thread-rolling process. From the experimental validation, they could acquire the successful thread shape with precise dimension[32].

1.3 Objective and scope of study

The objective of this study is to design the integrated manufacturing process of bolts with Al6061 alloy which can be used to fasten offshore platforms. The 6xxx series of aluminum alloys are commonly used in marine applications in which low specific weight materials, high quality mechanical properties, and high resistance to corrosion are desired[3]. Al6061 is a typical alloy of them which are age hardenable, and usually heat-treated to T6 condition in order to develop adequate strength[33]. The proposed scheme includes the theoretical design and numerical study for the heading, trimming, and thread-rolling process. In the theoretical design, the initial rod diameter and the range of the penetration depth in the thread-rolling process were calculated according to the screw standards and geometric relation. Then, the dimensions of the initial workpiece for the heading process were obtained using the volume-constancy law. Considering the process limitations to predict the defects, the number of stages was set. Subsequently, preform was determined by using the design rule in the heading process. Finally, in order to determine the feasibility of the designed heading process, the slab method was applied to predict the forming load. Based on the theoretical design, the FE-analysis for the heading, trimming, and thread-rolling processes was conducted. In order to investigate the defects and fracture phenomena, the ductile fracture criterion was applied during the heading and trimming processes. In addition, the Taguchi method was used to optimize the trimming and thread-rolling processes with the set of design parameters, such as the penetration depth, transfer velocity, and revolutions per minute in the thread-rolling process, and the blade radius, land width, and stop distance in the trimming process, respectively. To validate the proposed design method, the forming experiments of the Al6061 alloy M12 hexagonal bolt for fastening offshore platforms were performed.

2. Theoretical design of Al6061 alloy bolts manufacturing process

2.1 Procedures for theoretical design

Fig. 2 demonstrates the procedure for the theoretical design employed when manufacturing Al6061 alloy bolts. The first step is to design the layout of the entire process. Subsequently, the initial rod diameter and the range of penetration depths are calculated in the thread-rolling process. For the heading process, the calculation of the initial workpiece dimensions formed into the head section, the prediction of defects, the determination of the number of stages, and the preform design are conducted in turn. For the profile at each stage of multi-stage forging, process limitations are computed respectively. Finally, the forming load is analyzed by using the slab method in order to confirm the process feasibility.

The schematic illustration of the integrated manufacturing process of Al6061 alloy bolts is shown in Fig. 3. The integrated manufacturing process for aluminum bolts involves T0 heat treatment, heading, trimming, thread-rolling, and T6 heat treatment. In industrial practice, materials of the 6xxx series age naturally at room temperature, and the hardness of the material increases, causing a reduction in formability[34]. Therefore, the aluminum alloy coil, which is a raw material, is annealed to improve the workability and formability. Generally, the forging process for the bolt heading is classified into two groups according to the type of die, namely closed forging and free forging. In free forging, the trimming process is necessary to shape the head section, so the material loss by chips is inevitable. However, owing to the simple material deformation, it is beneficial to the component properties and forging load. On the contrary, closed forging has an advantage in that the product

can be formed by a single forging process, helping to reduce the cost of the process, but when the corner portion is filled, the load increases sharply[35,36]. The high forging force can cause significant failure, plastic deformation, and the wearing of dies, and it is thus an essential factor to be considered when designing the process[37]. Therefore, in this study, the free forging process is selected considering the tool life and capacity of the cold former for the prototype production. Following the bolt heading, T6 heat treatment is performed to remove the residual stress generated during the heading, and to improve the mechanical properties[38]. Finally, the shank of the Al6061 alloy bolts is fabricated by the thread-rolling process.

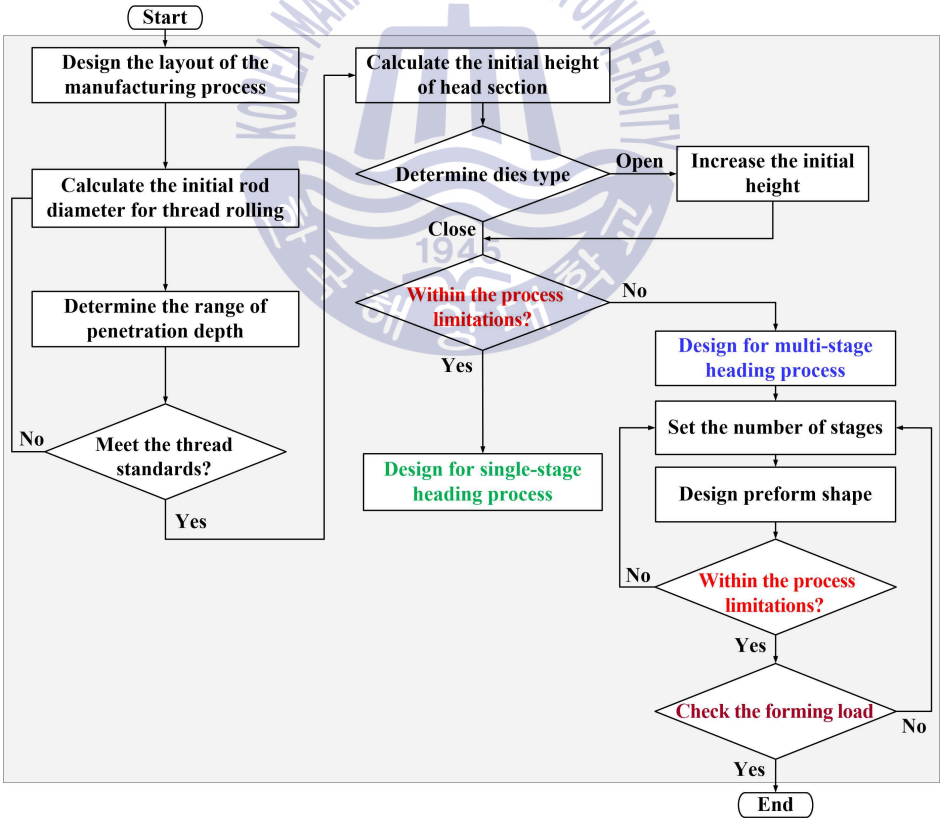

Fig. 2 Flow chart for theoretical design of cold heading and thread-rolling

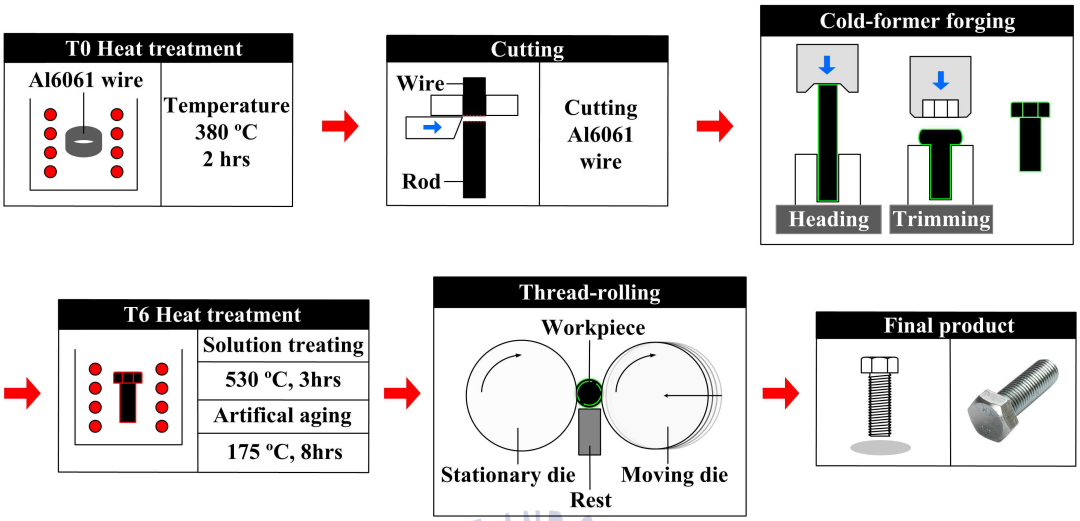

Fig. 3 Schematic illustration of Al6061 alloy bolt manufacturing process

2.2 Process design for thread-rolling

2.2.1 Calculation of initial diameter in thread-rolling process

The initial diameter of the workpiece in the thread-rolling process is an important parameter because it directly affects the accuracy of the screw-thread dimensions and the surface defects. If the initial diameter is small during thread-rolling, the height of the produced thread becomes low. On the other hand, the large initial diameter causes the crack to occur within the inside of the thread part due to a high level of tensile stress[27]. In general, the initial diameter in thread-rolling is determined based on the effective diameter of the screw. Fig. 4 displays the profile of the screw, and the effective diameter (d_2) can be calculated from Eq. (1) as follows[22]:

$$d_2 = d - 2 \times \frac{3}{8} h = d - \frac{3\sqrt{3}}{8} P \tag{1}$$

where d, h, and P are the outer diameter, height, and pitch of the screw, respectively. The screw dimensions according to ASME standards for M12 bolts are shown in Table 2[39]. By substituting the specifications of the M12 × 1.75 screw into Eq. (1), the initial diameter obtained is 10.75 mm.

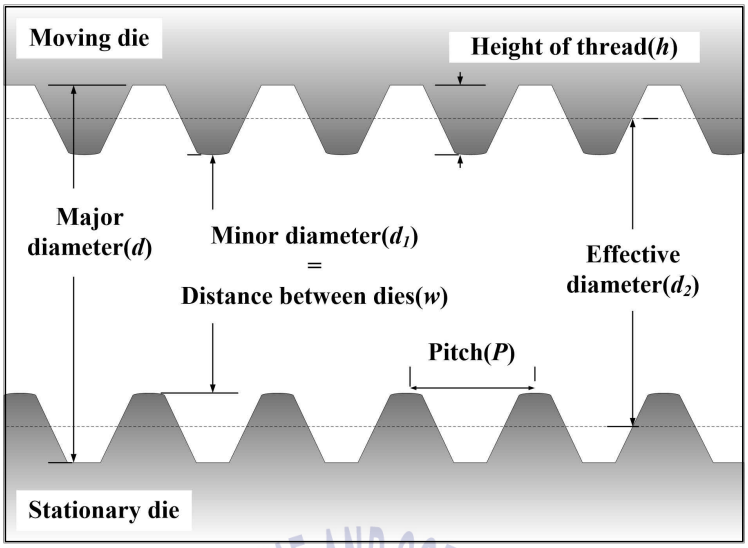

Fig. 4 Profile of the screw

Table 2 Screw dimensions according to ASME standards for M12 bolt

(unit: mm)

Basic thread designation	Pitch	Major diameter		Effective diameter	
		Max.	Min.	Max.	Min.
M12	1.750	11.966	11.701	10.829	10.679

2.2.2 Determination of penetration depth

The penetration depth (*PD*) of the thread-rolling dies is an important factor that influences the shape of the thread in the thread-rolling process. Fig. 5 shows the description of the PD of the thread-rolling dies. The PD is determined based on the initial diameter and the distance between thread-rolling dies. As shown in Fig. 4, the distance (*w*) between the

thread-rolling dies is identical to the minor diameter (d_1) of the thread. The smaller the distance between the thread-rolling dies, the better the formability of the screw threads. However, when the distance is too narrow, the dimensions of the major diameter cannot exceed a certain dimension ($w + 2h$), even if the material completely fills the cavity of thread-rolling dies. Considering these characteristics, the range of the distance between thread-rolling dies required to satisfy the standards for screws can be expressed by the following geometric relation[22]:

$$d_{\min} - 2h \le w \le d_0 - h \tag{2}$$

where d_{min} is the minimum value of the major diameter according to the screw standards, w is the distance between the dies, and d_0 is the initial workpiece diameter. Once the range of the distance between the dies is set, the range of the major diameter and the PD can be determined. Then, the PD is used as a design parameter in the optimization step for the thread-rolling process. Table 3 gives the calculation results of the initial diameter of the M12 bolt, distance between the dies, major diameter of the screw, and the PD. As can be seen from the above results, a product having a major diameter larger than the initial diameter is obtained after thread-rolling. This is because the material bulges up by the volume pressed by the dies during the thread-rolling process and forms threads, which is a singular point of the thread-rolling process compared with the conventional cutting process.

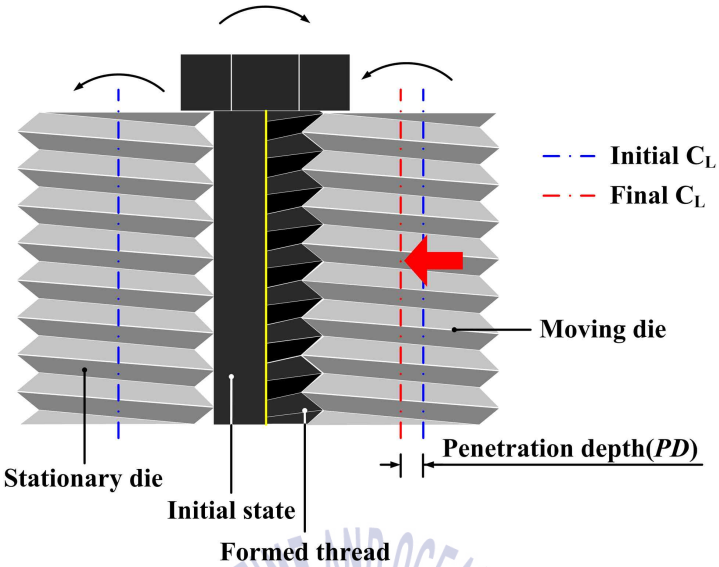

Fig. 5 Description of penetration depth

Table 3 Results of calculation for M12 screw profile

(unit: mm)

Initial diameter	Distance between dies		Major diameter		Penetration depth	
	Max.	Min.	Max.	Min.	Max.	Min.
10.750	9.670	9.560	11.818	11.708	1.190	1.080

2.3 Process design for heading

2.3.1 Determination of initial height of head section

As the first step of the heading process design, the initial height of the head part to be formed into the hexagonal shape should be calculated. To do this, information on the final shape of the bolt head and the initial diameter for the heading process is required. Table 4 and Fig. 6 show the M12 hexagonal bolt specification and dimensions with reference to the ASME standards[40]. In practice, the initial diameter for the heading process is determined based on the initial diameter of the thread-rolling process. In the present stage, it is assumed that the head part can be formed by a single process. Therefore, the initial diameter in the heading process is set to be 10.7 mm so that the workpiece can be easily inserted into the bottom die of the heading process. Considering the trimming process, the calculated initial height of the head is found to be 34.5 mm by applying the volume constancy law with the information on the initial diameter and the final shape of the bolt head.

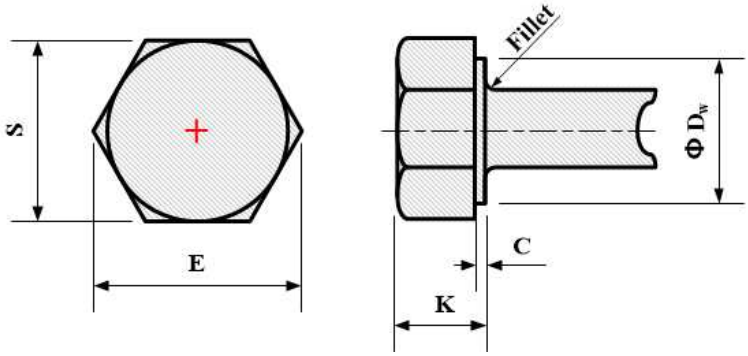

Fig. 6 Specification of M12 hexagonal bolt with reference to ASME standards

Table 4 Dimensions of M12 hexagonal bolt with reference to ASME standards

(unit: mm)

S		E		K		C		D_w	Fillet
Max.	Min.	Max.	Min.	Max.	Min.	Max.	Min.	Min.	Min.
18.00	17.57	20.78	19.68	7.76	7.24	0.6	0.3	16.6	0.6

2.3.2 Theoretical prediction of defects and setting of the number of process stages

On the basis of the preliminary design information above, the occurrence of defects such as buckling and cracks during the heading process is theoretically predicted and the number of process stages is determined. According to the previous studies[35,41], the design rules for upsetting are summarized as follows (See Fig. 7):

1) The length of the unsupported stock that can be gathered or upset in one blow without buckling is not more than 2.3 times the diameter of the bar.

2) A length of bar more than 2.3 times the diameter of the bar can be successfully upset in one blow, provided the diameter of upset is restricted to not more than 1.5 times the diameter.

3) For an upset requiring more than 2.3 times the diameter of stock in length and for which the diameter of the upset is 1.5 times the diameter of the bar, the amount of unsupported stock length beyond the face of the die must not exceed the diameter of the bar. If, however, the diameter of the die cavity is reduced below 1.5 times the diameter of the stock, then the length of unsupported stock beyond the face of die can be correspondingly increased. If the cavity diameter is not greater than 1.25 times the diameter of the stock, then the amount of stock beyond the face of the die may be

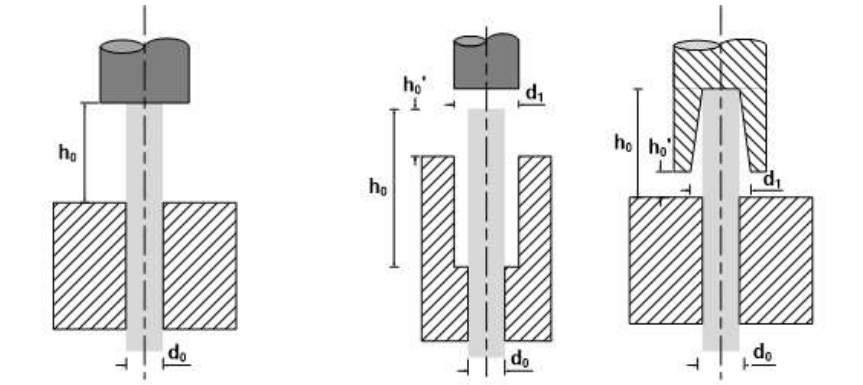

Fig. 7 Design rules for upsetting

increased to a maximum of I.5 times the diameter of the bar.

Since, in this study, the free forging is conducted, the first design rule was considered and a process limitation, namely the upset ratio (s), was defined as follows:

$$s = \frac{h_0}{d_0} (s \leq 2.3) \tag{3}$$

where h_0 is the initial head height, and d_0 is the diameter of the workpiece.

The upset ratio is a factor that affects the buckling of the workpiece, and is expressed as a ratio of the diameter to the height of the head section. It

is virtually independent on the material, and thus considered to be applicable for aluminum alloy bolt forming as well.

Even though, the design rules above are practical and have been widely used in forging industry, there is the limit to consider the formability which depends on the material properties. Thus, the second process limitation, which is called upset strain (ϕ_p), was adopted with the reference to the earlier study[42].

$$\phi_p = \ln \frac{h_1}{h_0} (\phi_p \leq 1.6 \sim 2.1) \tag{4}$$

where h_0 is the initial head height, and h_1 is the head height after the upsetting process.

The upset strain, which is provided as a ratio of the heights of the head before and after the process, represents the formability of the material. The ranges in parentheses in Eqs. (3) and (4) indicate the values in which the heading process can be performed in a single operation.

Using Eqs. (3) and (4), the calculation results indicate that the buckling is expected during the single operation owing to the excessive upset ratio of 3.2, and therefore, the process design is modified to multi-stage heading process. The newly designed heading process consists of preforming, 1st upsetting and 2nd upsetting, considering the 4-stage cold former for prototype production, where the trimming process is also conducted. Based on the modified design, the initial diameter for the heading is changed from 10.7 mm to 10.58 mm, and the initial height of the head part is also changed from 34.5 mm to 36 mm according to the target volume.

2.3.3 Preform design for heading process

The design rule proposed by K. Lange (1985)[43] was applied to the design of the preform in the heading process, which has been typically carried out by trial-and-error in industry. Fig. 8 provides design rule to design the preform shape in bolt manufacturing. By interpolating the dimensions within the range of the design rule, the preform was designed considering the volume ratio of the head section of the workpiece to the inner cavity of the punch. Fig. 9 illustrates the profile at each stage of the cold-former forging process, including the preform for the heading process designed in this section.

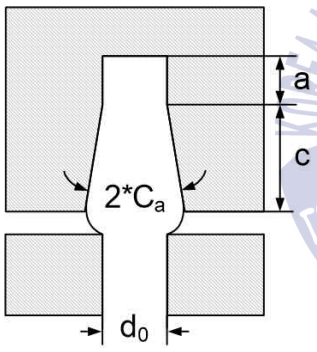

Upset Ratio	Cone Angle	Guide Length	Length Portion of cone
$s=h_0/d_0$	$2*C_a$	a	c
2.5	15	$0.6d_0$	$1.37d_0$
3.3	15	$1.0d_0$	$1.56d_0$
3.9	15	$1.4d_0$	$1.66d_0$
4.3	20	$1.7d_0$	$1.56d_0$
4.5	25	$1.9d_0$	$1.45d_0$

Fig. 8 Design rule for preform shape

(unit: mm)

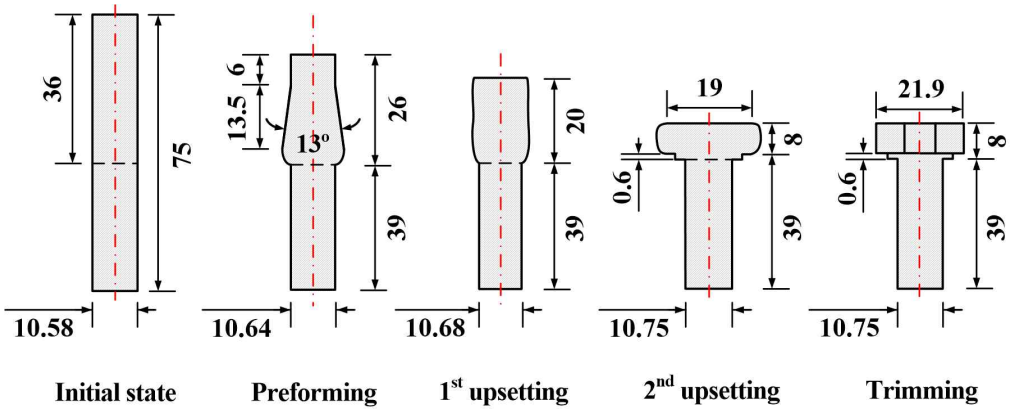

Fig. 9 Profile at each stage of the cold-former forging process

Once the design of intermediate shapes for multi-stage heading was completed, then process limitations at each stage should be calculated to check the occurrence of defects during the process. For upsetting with taper dies, it is necessary to determine an equivalent diameter in order to apply the above process limitations. One method is to used the arithmetic mean of the top and bottom cavity diameters to determine the upset ratios. However, in this case, tapered dies offer no advantage over cylindrical cavities in the amount of material that can be formed in one operation. Since buckling is dependent on the inertia moment of a section, it would seem preferable to use inertia moment as a means of determining an equivalent diameter for calculations of the upset ratio. The equivalent mean diameter($d_{m,i}$) is calculated from the arithmetic mean of inertia moments of end sides of tapered shape as follows[41]:

$$d_{m,i} = (\frac{d_a^4 + d_c^4}{2})^{1/4} \quad (5)$$

where d_a and d_c are diameters of the tapered die cavity.

For the 1st upsetted shape, it is assumed that the shape is identical to a cylinder, thus the equivalent diameter was calculated by volume constancy law. Table 5 shows the calculation results of process limitations at each stage and the process design of multi-stage heading seems to be appropriate, for the values are within the allowable ranges.

Table 5 Calculation results of process limitations

	Initial (Single stage)	Modified (Multi-stage)		
Stage	Single upsetting	Preforming	1st upsetting	2nd upsetting
d_0 [mm]	10.70	10.58	12.46 ($d_{m,i}$)	14.19
h_0 [mm]	36.0	30.0	26.0	20.0
h_1 [mm]	8.0	20.0	20.0	8.0
s	3.36	0.95	0.48	0.85
φ_p	1.50	0.41	0.26	0.92

2.3.4 Forming load prediction by slab method

As a final stage in the design of heading process, the forming load was predicted by slab method to determine the process feasibility. Slab method analysis is useful tool in estimating the force during the various metal forming processes. In particular, load evaluation of an axisymmetric homogeneous open -die upset, typical one of free forging processes, is given as (See Fig. 10)[44]:

$$L = \frac{\pi}{4} d_1^2 \sigma_f \left(1 + \frac{m d_1}{3\sqrt{3}\, h_1}\right) \tag{6}$$

$$\sigma_f = K\left(\ln \frac{h_0}{h_1}\right)^n \tag{7}$$

where d_1 is the final upset head diameter, σ_f is the material flow stress, m is the shear friction factor, h_1 is the final height of upset head, h_0 is the initial height of workpiece to be upset, K is the strength coefficient and n is the strain hardening exponent.

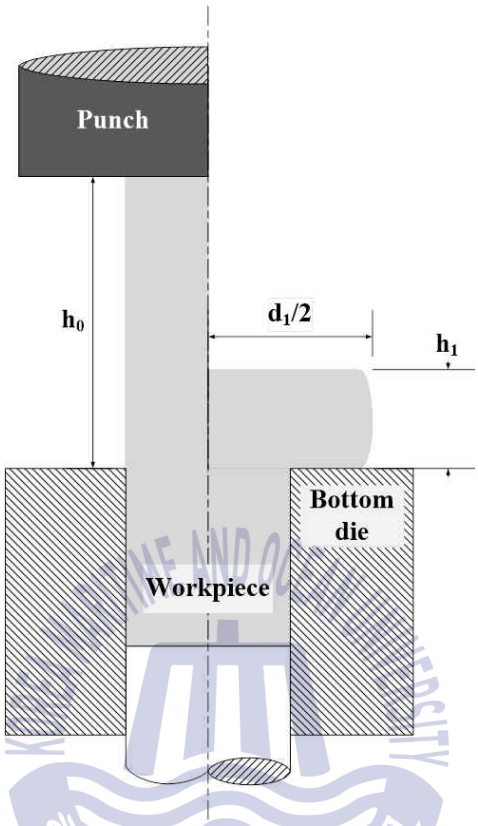

Fig. 10 Axisymmetric homogeneous open-die upset

However, this formula is valid only for an open-die upset, and is therefore not applicable to predict the load for an closed-die upset such as the preforming designed in this study and even the final upsetting whose dies has somewhat geometrical complexity due to the tapered upper part and washer face as well. Thus, the modified slab method[45] was applied to predict the forming load for the multi-stage heading process.

Fig. 11 illustrates the preforming process for the application of modified slab method. Because the material flow in the tapered dies is restricted by the cavity, less workpiece volume deforms than does in an open-die upset.

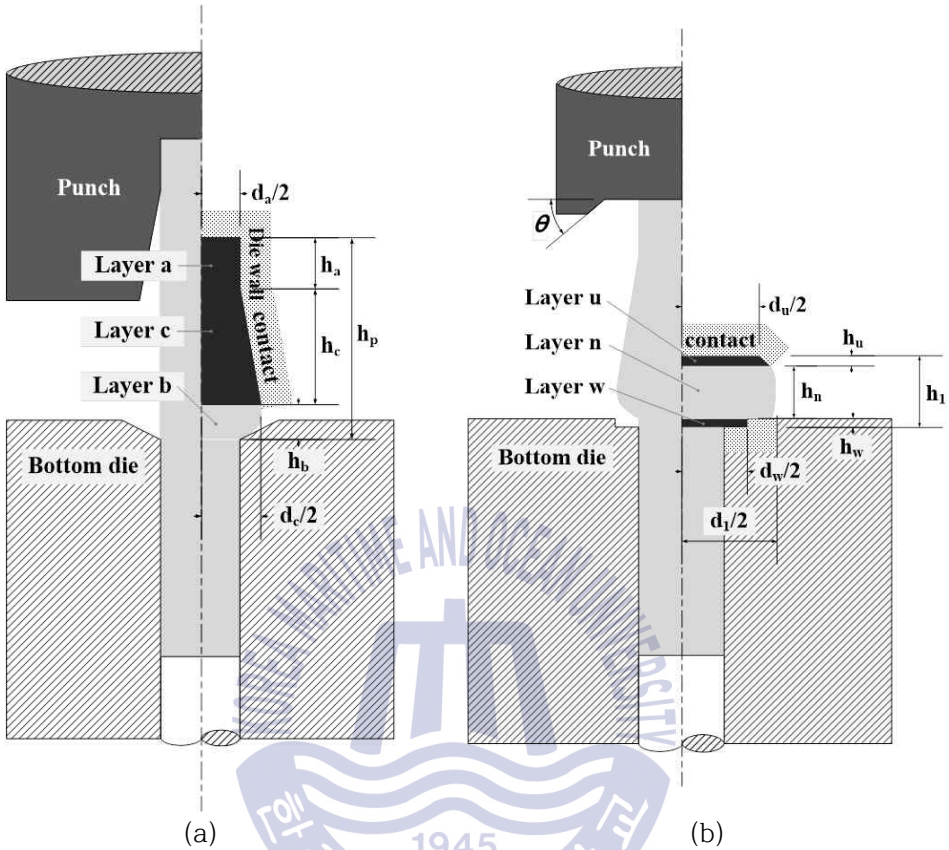

Fig. 11 Application of modified slab method: (a) preforming, (b) upsetting

Hence, a modification to the conventional slab method is made to account for the reduced deformation zone when trying to predict the forging load.

The maximum forging load occurs at the end of the upset stroke. At the end of the stroke, the head part can be divided into three distinct layers by similar deformation characteristics as shown in Fig. 11(a). The top and middle layer (layer a and layer c) are in contact with the die wall, and assumed to not deform further, which menas it can be considered to undergo rigid-body motion. The bottom layer (layer b), however, continues to deform because they are not restricted by the die wall. To compute the actual forging load

using the modified slab method, it is important to consider only the bottom layer.

In Eqs. (6) and (7), the only geometrical variables required to predict the forging load are the final diameter, d_1, and the initial and final heights of head part, h_0 and h_i. Therefore, these variables must be corrected to reflect only the bottom layer. Eqs. (6) and (7) are modified and given as below:

$$L = \frac{\pi}{4} d_{m,b}^2 \sigma_f (1 + \frac{m d_{m,b}}{3\sqrt{3}\, h_b}) \tag{8}$$

$$\sigma_f = K(\ln \frac{h_{0,b}}{h_b})^n \tag{9}$$

where $d_{m,b}$ is the equivalent mean diameter of bottom layer, h_b is the final height of bottom layer, $h_{0,b}$ is the initial height corresponding to the final height h_b, σ_f is the material flow stress, m is the shear friction factor, K is the strength coefficient and n is the strain hardening exponent.

The volume constancy principle was used to find the values of $d_{m,b}$ and $h_{0,b}$ as shown in Fig. 12. Assuming the bottom layer is identical to the equivalent cylinder with the diameter $d_{m,b}$, the initial height $h_{0,b}$ is then found using the following equations.

$$d_{m,b} = \sqrt{\frac{4 V_b}{\pi h_b}} \tag{10}$$

$$h_{0,b} = \frac{4 V_b}{\pi d_0^2} \tag{11}$$

$$V_b = V_p - (V_a + V_c) = \frac{\pi}{4}\left\{d_0^2 h_p - (d_a^2 h_a + \frac{1}{3}h_c(d_a^2 + d_c^2 + d_a d_c))\right\} \quad (12)$$
$$= \frac{\pi d_m^2}{4} h_b = \frac{\pi d_0^2}{4} h_{0,b}$$

where V_p, V_a, V_b and V_c are volumes of preform, layer a, layer b and layer c, respectively, and h_p, h_a, and h_c is the height of preform, top layer, and middle layer, respectively. The volume of V_c is computed using the formula for a truncated cone.

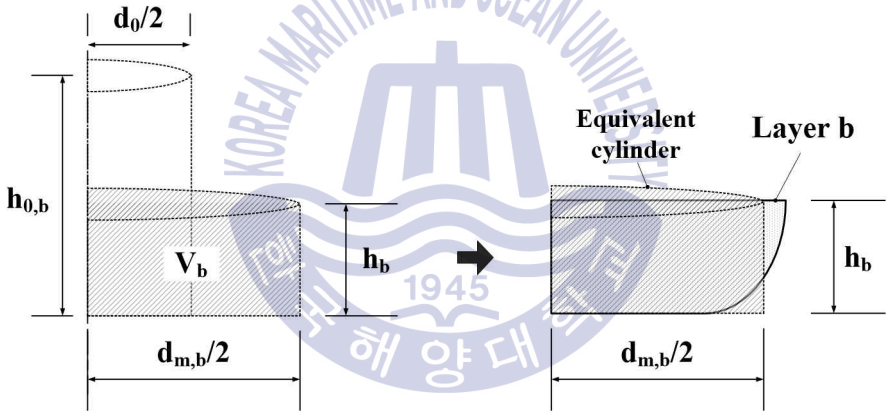

Fig. 12 Volume constancy principle using equivalent cylinder

In the same manner as the preforming, the forged head of the final upsetting(i.e. 2nd upsetting) is divided into three parts: upper head part (layer u), net upsetted part (layer n), and washer face part (layer w) as shown in Fig. 11(b). At the end of stroke, only the material of layer n is deformed while the materials of layer u and layer w are captured by the cavity of the punch and washer face of bottom die, respectively. The predicted forging load

can be computed using the Eqs. (13) and (14) below:

$$L = \frac{\pi}{4} d_1^2 \sigma_f \left(1 + \frac{m d_1}{3\sqrt{3}\, h_n}\right) \tag{13}$$

$$\sigma_f = K(\bar{\epsilon}_p + \ln \frac{h_p}{h_n})^n \tag{14}$$

where d_1 is the diameter of final upsetted head, h_n is the final height of net upsetted part, h_p is the height of preform, σ_f is the material flow stress, $\bar{\epsilon}_p$ is the mean effective strain by preforming, m is the shear friction factor, K is the strength coefficient and n is the strain hardening exponent.

The unknown variables in the load prediction formula are the diameter of final head d_1 and the height of net upsetted head h_n. The value of h_n can be found by using Eq. (15). Satisfying the volume constancy principle, a third-order equation in terms of d_1 is obtained as shown in Eq. (16). If the Eq. (15) is substituted into Eq. (16), the d_1 will be obtained as the cubic root of the Eq. (16). Finally, the predicted forging load can then be calculated using Eq (13) and (14) above.

$$h_n = h_1 - ((d_1 - d_u)/2\tan\theta + h_w) \tag{15}$$

$$V_p = \frac{\pi}{4}\left\{\frac{1}{3} h_u (d_u^2 + d_1^2 + d_u d_1) + d_1^2 h_n + d_w^2 h_w\right\} \tag{16}$$

3. FE-analysis of cold-former forging process

3.1 Conditions of FE-analysis in heading process

The FE-analysis was performed for the cold-former forging process, which consists of the heading and trimming, using DEFORM-2D. The stress-strain curve of Al6061-T0 acquired from the uniaxial tensile test is shown in Fig. 13. Considering the axisymmetric shape of the product, the two-dimensional (2D) FE-model was applied in the heading process, as shown in Fig. 14. The number of elements and nodes are 5,054 and 5,340, respectively. The punch speed is 100 mm/s, taking into account the cold-former specification used for the experiment. The friction factor (m) between the material and dies is set to 0.1[44]. Because there is no heat treatment process in multi-stage cold heading, the FE-analysis was executed continuously from the first stage to the final one.

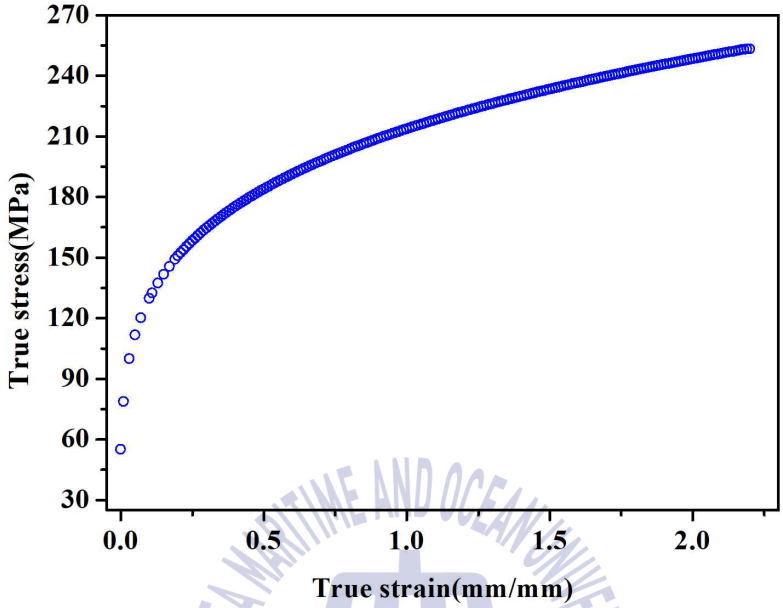

Fig. 13 Stress-strain curve of Al6061-T0

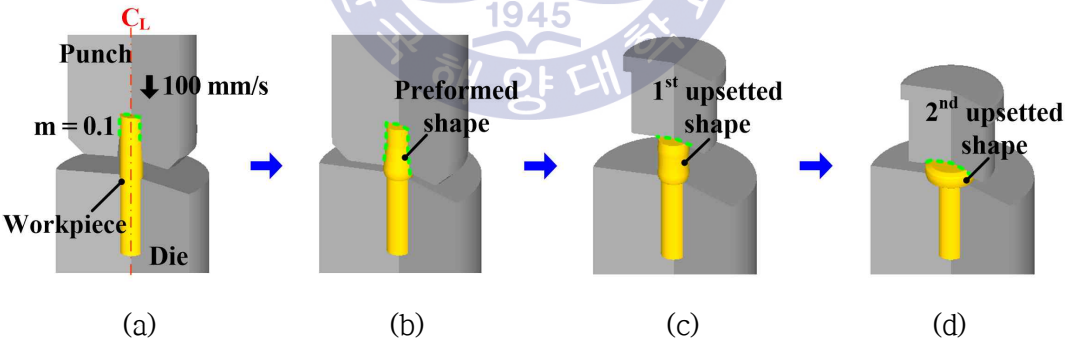

Fig. 14 2D FE-model of heading process: (a) initial state, (b) preforming, (c) 1st upsetting, (d) 2nd upsetting

3.2 Results of FE-analysis in heading process

Fig. 15 shows the FE-analysis results for each forging stage in the heading process. During the preforming, the deformation of the material was confined to the lower portion of the head owing to the internal shape of the punch cavity. In the 1st upsetting process, the top of the head where little deformation had taken place during the preforming was mainly forged. On the contrary, the lower part of the head where the work hardening occurred in the previous step was relatively less deformed. As a result of the 2nd upsetting process, the inhomogeneous deformation of the typical upsetting pattern, i.e., barreling owing to friction between the punch and the workpiece, was shown with the peak effective strain of 2.3.

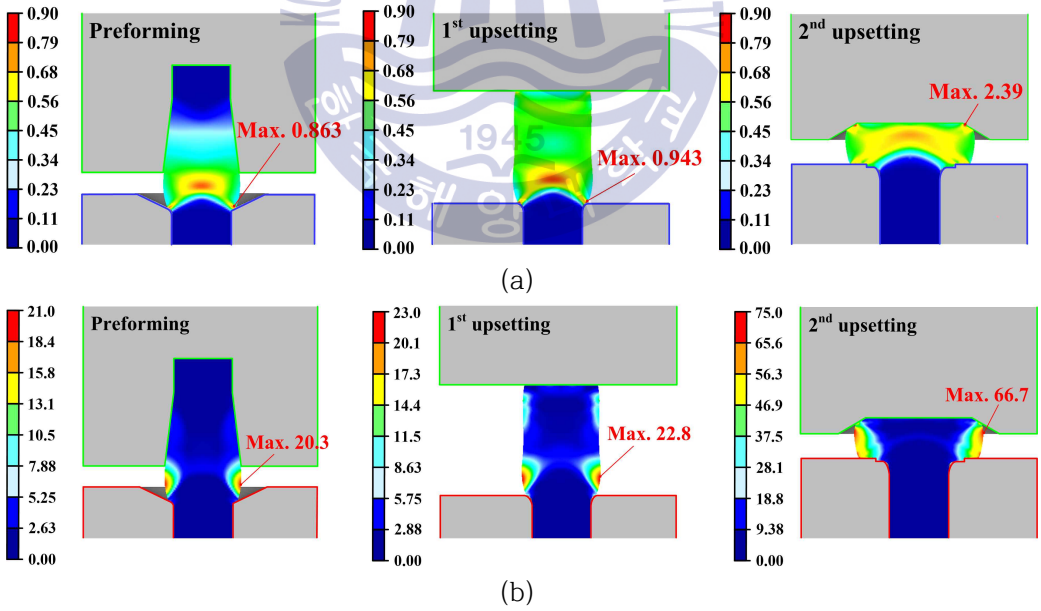

Fig. 15 FE-analysis results for each forging stage in the heading process: (a) effective strain distribution, (b) damage distribution

To predict the defects during the heading process, the ductile fracture criterion was used. There have been many theories for ductile fracture prediction. In the present study, the Cockcroft & Latham's criterion expressed by Eq. (17) was adopted because it is useful in designing the cold forging process in which the influence of the induced circumferential tensile stress on failure is dominant[46].

$$C_1 = \int_0^{\bar{\epsilon}_f} \sigma_{\max} d\bar{\epsilon} \tag{17}$$

where $\bar{\epsilon}_f$ is the fracture strain, $\sigma_{\max}$ is the maximum principal stress, ε is the equivalent strain, and C_1 is the damage value as the material constant. The rupture of the bolt head occurs when it exceeds C_1, which is the critical damage value according to the Cockcroft-Latham's ductile fracture criterion. By comparing tensile test results with FE-analysis results, the critical damage value of the Al6061-T0 material was determined to be 74.4. As shown in Fig. 15(b), a maximum damage value of 66.7 was observed after the final stage forging, which is lower than the critical one. Therefore, it is considered that the heading process, which was designed theoretically, can be performed without defects.

The predicted forming load by FE analysis is provided in Fig. 16. It was found that the preforming, 1st upsetting and 2nd upsetting processes require the forming loads of approximately 3.7 tons, 3.5 tons and 13.9 tons, respectively. As shown in Table 6, the predicted forming load by the slab method was in good agreement with the FE analysis results, proving its effectiveness. In addition, the cold-former used in the experiment (400 tons) appears to be appropriate for the bolt forming considering the capacity of the

cold-former must be larger than the sum of the maximum load at each stage[18].

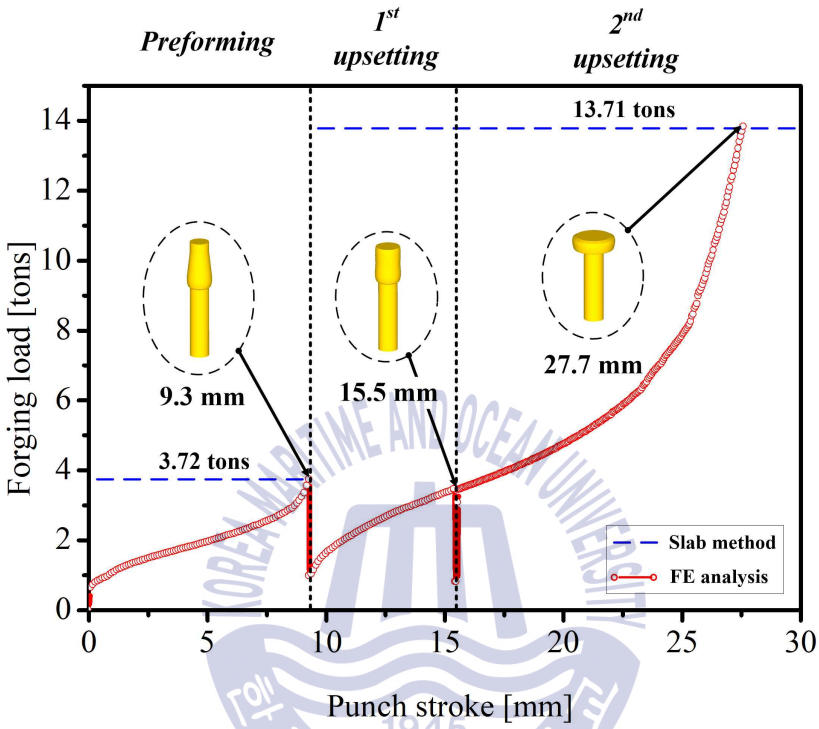

Fig. 16 Predicted forming load for heading

Table 6 Comparision of predicted forming loads by slab method and FE analysis

(unit: tons)

Process / Method	Preforming	Upsetting
Slab method	3.72	13.71
FE analysis	3.73	13.87

3.3 Design of experiment for trimming process

3.3.1 Taguchi method

The Taguchi method is one of design of experiment (DOE) techniques, which is applied to determine the optimum levels of the design parameters. The greatest advantage of the Taguchi method is to find out significant parameters in a shorter time period, reducing the experimental time and the cost. In other words, using analysis of variance (ANOVA) and signal to noise (SN) ratio, the effects of vital parameters on the response can be determined, and the best parameter levels for a given process can be identified from the selected parameter levels.

In Taguchi method, deviation between experimental and desired values is defined as loss function, which is further converted into SN ratio. In general, SN ratio characteristics are divided into three types written in Eqs. (18) – (20):

The-nominal-the-best characteristic,

$$SN = 10\log\left[\frac{\bar{y}}{S_y^2}\right] \tag{18}$$

The-smaller-the-better characteristic,

$$SN = -10\log\left[\frac{1}{n}\sum_{i=1}^{n} y_i^2\right] \tag{19}$$

The-larger-the-better characteristic,

$$SN = -10\log\left[\frac{1}{n}\sum_{i=1}^{n}\frac{1}{y_i^2}\right] \tag{20}$$

where $\bar{y}$, $\bar{S}_y^2$, n and y are the average of observed data, the variation of y, the number of observations, and the observed data or each type of the

characteristics, respectively.

Regardless of the category of the quality characteristic, a greater SN ratio corresponds to better quality characteristics. Therefore, the optimal level of the process parameters is the level with the greatest SN ratio.

The optimum process conditions are chosen according to the SN ratio, while the interaction between the process parameters is determined with the help of the variance analysis. ANOVA is a statistical method which is used to define the individual interactions into the test results of all the operating parameters. The equations relevant with analysis of variance are as follows:

$$SS_{total} = \sum_{i=1}^{N} \eta_i^2 - CT \tag{21}$$

$$SS_A = \frac{1}{m_A} \sum_{i=1}^{L_A} T_{A_i}^2 - CT \tag{22}$$

$$CT = \frac{T_{SN}^2}{N} \tag{23}$$

$$DOF_A = L_A - 1 \tag{24}$$

$$V_A = \frac{SS_A}{DOF_A} \tag{25}$$

$$P_A(\%) = \frac{V_A}{V_{total}} \times 100 \tag{26}$$

where SS_{total} is total squared sum of SN ratios, η is SN ratio of the i^{th} experiment, N is total number of experiments, CT is corrective term, SS_A is squared sum of SN ratio of the parameter A, L_A is number of levels of parameter A, T_{Ai} is sum of SN ratios when parameter A is at i level, m_A is number of repetitions of experiments for A, T_{SN} is sum of SN ratios, DOF_A is degree of freedom of each parameter, V_A is the mean square of A parameter, V_{total} is sum of mean square for all experiments, and P_A is contribution of parameter A to the process, respectively.

3.3.2 Parameter design for the Taguchi method

For the application of Taguchi method, three design parameters and two objective functions are defined. Fig. 17 displays descriptions of design parameters such as the blade radius (BR) of punch, land width (LW) of bottom die, and stop distance (SD) between the punch and the bottom die.

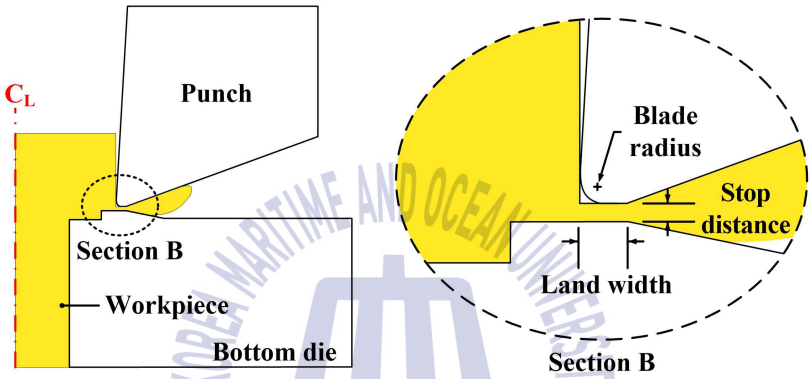

Fig. 17 Descriptions of design parameters in trimming process

Contrary to the sheet trimming, which is processed in a single stage, the bolt trimming proceeds in two sequences, i.e., 1st sequence by the punch and 2nd sequence by the knockout pin, as shown in Fig. 18[15]. Besides, as can be seen in Fig. 19, when the edges of the trimming punch and the land of the bottom die are aligned (LW = 0), a relatively large fracture zone occurs in the middle of the sheared plane, leaving a large crack trace, which reduces the shear surface quality[19]. It is interesting to note that the tensile hydrostatic stress is observed in the shear zone between punch and workpiece in Fig. 20. It is believed that when a compressive hydrostatic stress is applied during trimming, crack propagation is delayed and the effective shear section increases[14]. In the case of bolt trimming, it is necessary to secure a sound shear cross section to the final shearing while suppressing the occurrence of

cracks by giving a reaction force in the bottom die against the trimming load. For this reason, the LW of the bottom die was offset by 0.5 mm, 1.0 mm, and 1.5 mm from the shear zone of the bolt head[19]. The BR of the punch and the stop distance between the punch and the bottom die were determined by referring to previous research results[14,15]. Table 7 and Table 8 display the design parameters and $L_9(3^3)$ orthogonal array table generated by design parameters with three levels.

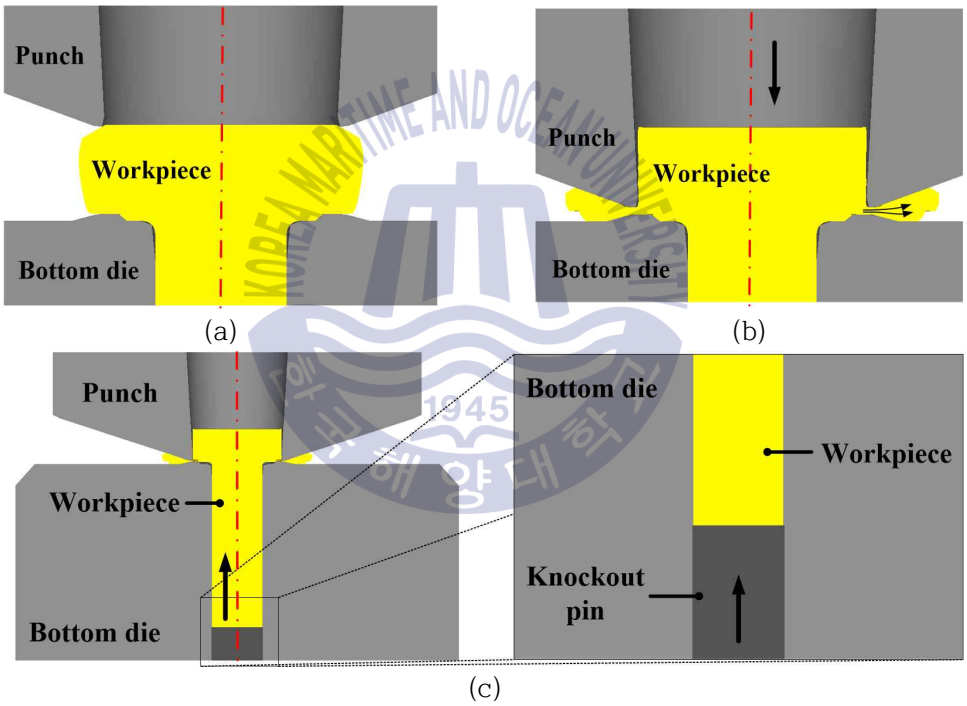

Fig. 18 Schematic illustration of trimming process: (a) Initial state (b) 1st sequence (c) 2nd sequence

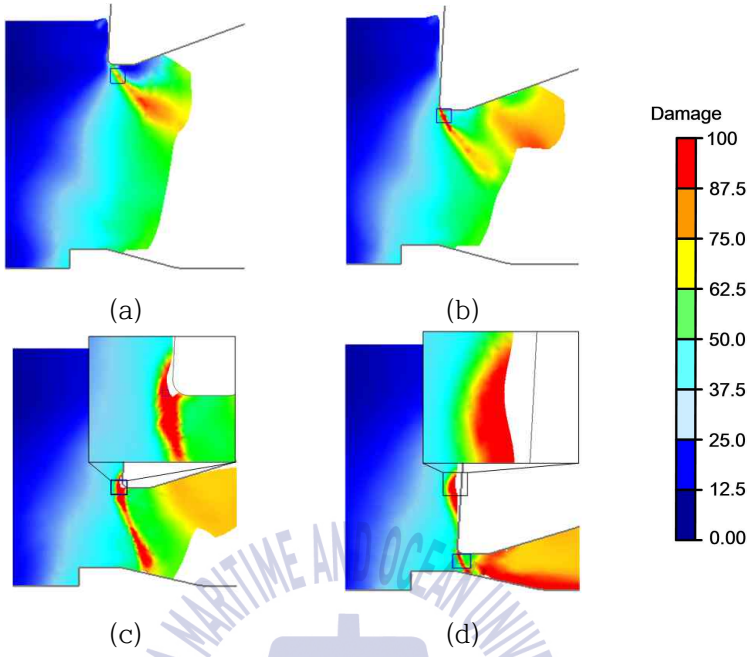

Fig. 19 Damage distribution during crack propagation in trimming process: (a) 16.6% stroke (b) 39.1% stroke (C) 66.2% stroke (d) 98.0% stroke

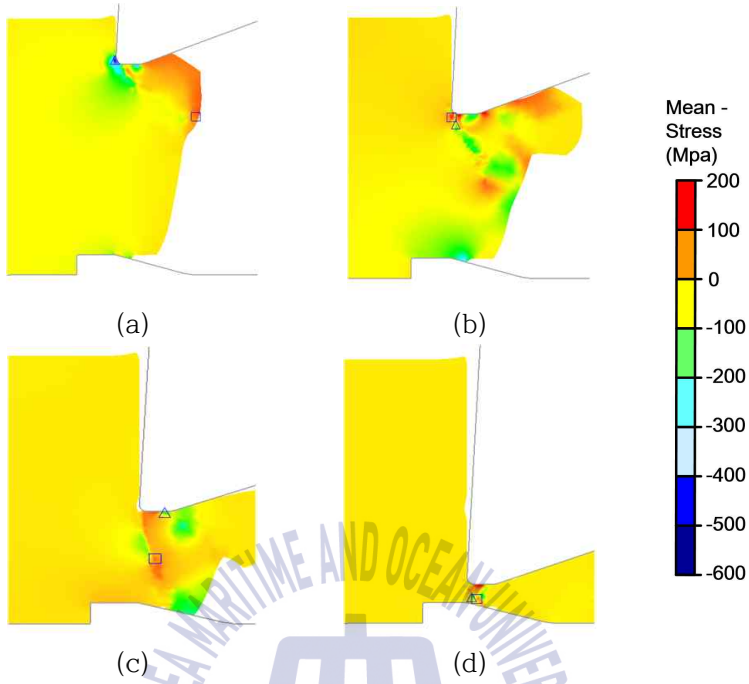

Fig. 20 Mean stress distribution during crack propagation in trimming process: (a) 16.6% stroke (b) 39.1% stroke (C) 66.2% stroke (d) 98.0% stroke

Table 7 Design parameters and their levels for trimming process

(unit: mm)

Parameters	Level 1	Level 2	Level 3
Blade radius (BR)	0.2	0.3	0.4
Land width (LW)	0.5	1.0	1.5
Stop distance (SD)	0.25	0.5	0.75

Table 8 $L_9(3^3)$ orthogonal array table for trimming

No. of simulation	BR	LW	SD
1	0.2	0.5	0.25
2	0.2	1.0	0.50
3	0.2	1.5	0.75
4	0.3	0.5	0.50
5	0.3	1.0	0.75
6	0.3	1.5	0.25
7	0.4	0.5	0.75
8	0.4	1.0	0.25
9	0.4	1.5	0.50

To investigate the effects of the design parameters on the shear surface quality and trimming load, two objective functions, i.e., shape defects (DF_{shape}) and peak trimming load ($Load_{peak}$), are specified as presented in Fig. 21. The shape defects (DF_{shape}) is expressed as following below[19]:

$$DF_{shape} = w_R A_R + w_U A_U + w_B A_B \tag{27}$$

where A_R, A_U and A_B are the area of the roll-over, under-filling and burr along the shear surface, and w_R, w_U and w_B are the weight of roll over, under-filling and burr, respectively. Considering the influence on shear surface quality, weights of shape defects were determined as follows: w_R = 0.2, w_U = 0.3, and w_B = 0.5.

From the punch stroke-trimming load curve (See Fig. 21(b)), it is observed that the multiple sets of shear and fracture occur during the bolt trimming. According to the punch stroke, the load is gradually reduced with periodical fluctuations. Therefore, the peak-trimming load is generated at the end of the first shearing stage. The goal of this research was to minimize the DF_{shape} and $Load_{peak}$ in the trimming process. Therefore, the signal to noise (SN) ratio was calculated by applying the loss function of the-smaller-the-better characteristics using Eq. (19).

In the same manner as the heading process, the Cockcroft & Latham criterion was adopted to investigate the fracture phenomena during the trimming process because it is easy to utilize and relatively accurate for the bolt trimming process[15,47].

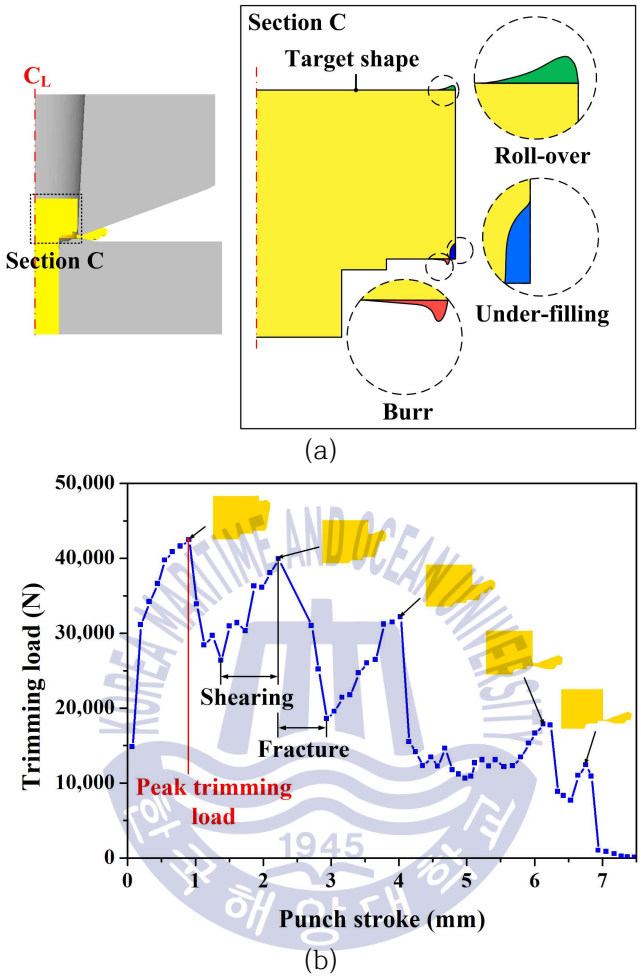

Fig. 21 Descriptions of objective functions: (a) DF_{shape}, (b) $Load_{peak}$

3.4 Conditions of FE-analysis in trimming process

Following the heading process, it is necessary to fabricate the forged head section into a hexagonal shape, which is called the trimming process. The FE-analysis was carried out to investigate the deformation behavior in trimming process using DEFORM-2D. During trimming process, the shape defects occur non-uniformly along the sheared section, making quantitative measurements very difficult[12]. Therefore, referring to the previous study[14], a two-dimensional analysis was performed on the cross section A-A' where the maximum scrap of the material is generated (See Fig. 22, 23) in order to reduce the analysis time and to facilitate the comparison between the analysis results. A finer mesh to the shear zone is applied so that the accuracy of the analysis for the shear and fracture behavior can be improved. As a result, 8,494 nodes and 8,230 elements were generated, respectively. The friction factor (m) between the workpiece and punch is set to be 0.1 with reference to the previous study[17]. The deformation history generated in the forging process was imposed on the material. Owing to the identical cold-former specification, the speed of the trimming punch was the same as the speed of the punch for the heading process.

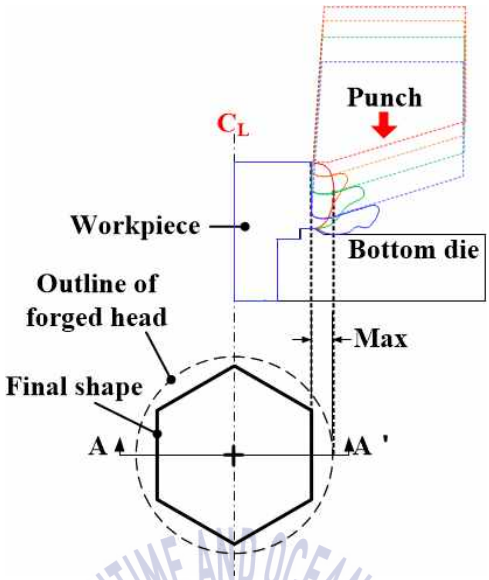

Fig. 22 Description of the cross-section for FE-analysis

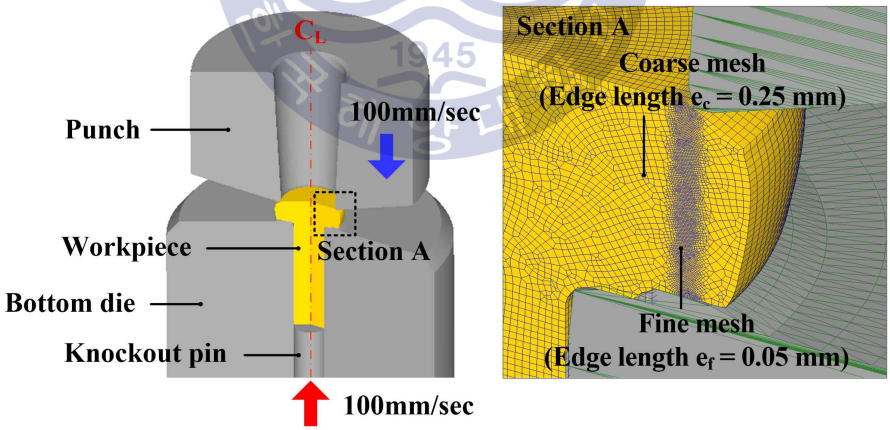

Fig. 23 2D FE-model of trimming process

3.5 Results of FE-analysis in trimming process

Table 9 and Table 10 show analysis results based on the $L_9(3^3)$ orthogonal array and SN ratios. In order to study the significance of the design parameters towards objective functions, analysis of variance (ANOVA) was performed. It was found that the effect of the BR (64.1%) on the DF_{shape} is the greatest, followed by the SD (22.2%) and the LW (13.6%). In the case of the $Load_{peak}$, it is mainly influenced by the BR (99.8%), with the remaining parameters having a very small effect. The results of analysis of variance are shown in Table 11 and Table 12.

To select the optimal levels of design parameters, the means of the SN ratios were calculated and plotted in Fig. 24. The highest values were selected for each design parameter. The process condition in which the SN ratio is a maximum for the DF_{shape} is a BR of 0.2 mm, LW of 1.0 mm, and SD of 0.25 mm. The SN ratios of the $Load_{peak}$ show the tendency to be inversely proportional to the increase of the BR. This is because as the BR increases, the contact surface of the punch and material become larger, resulting in an increase in the forming load. Therefore, the optimum process condition for the $Load_{peak}$ is a BR of 0.2 mm, LW of 1.5 mm, and an SD of 0.75 mm. The optimum process conditions for the LW and SD were determined based on the DF_{shape} with relatively high sensitivity. Thus, the optimum condition of the trimming process derived from the results of FE-analysis by the Taguchi method is as follows: BR = 0.2 mm, LW = 1.0 mm, and SD = 0.25 mm.

Table 9 Results of FE-analysis for DF_{shape}

No. of simulation	DF_{shape} [mm^2]	SN ratio
1	0.0120	38.4164
2	0.0100	40.0000
3	0.0460	26.7448
4	0.149	16.5363
5	0.0490	26.1961
6	0.0300	30.4576
7	0.0580	24.7314
8	0.0420	27.5350
9	0.188	14.5168

Table 10 Results of FE-analysis for $Load_{peak}$

No. of simulation	$Load_{peak}$ [N]	SN ratio
1	42,414	-92.5502
2	42,414	-92.5502
3	42,290	-92.5248
4	43,108	-92.6912
5	43,079	-92.6853
6	43,102	-92.6899
7	44,056	-92.8801
8	43,980	-92.8651
9	44,068	-92.8825

Table 11 Results of analysis of variance for DF_{shape}

Parameter	SS	DOF	V	P [%]
BR	229.8	2	114.9	64.1
LW	48.80	2	24.40	13.6
SD	79.53	2	39.76	22.2

Table 12 Results of analysis of variance for $Load_{peak}$

Parameter	SS	DOF	V	P [%]
BR	0.168	2	0.084	99.8
LW	0.000115	2	0.000057	0.0684
SD	0.000190	2	0.000095	0.112

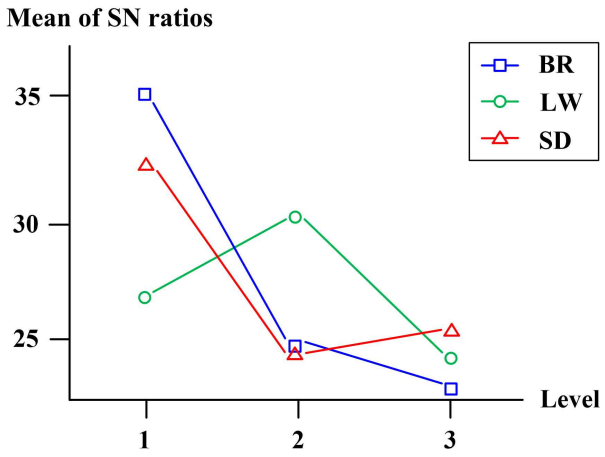

(a)

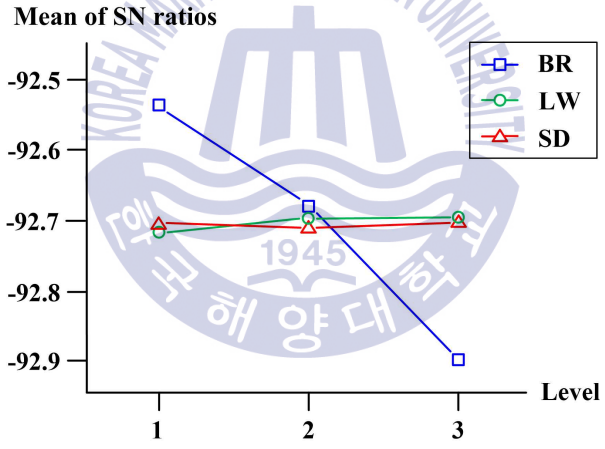

(b)

Fig. 24 Main effect plots on objective functions in trimming process: (a) DF_{shape}, (b) $Load_{peak}$

The FE-analysis was performed for the optimum process condition. Fig. 25 and Fig. 26 illustrate the distribution of the damage and hydrostatic stress on the sheared plane during the trimming process, respectively. Although a high

local damage value occurred in the middle of the shear section, critical shape defect, which was found in the initial FE-analysis (See Fig. 19(c)), was not observed. This may be owing to the compressive hydrostatic stress acting on the shear zone between the punch and the workpiece. In addition, as in the previous study[15], final shearing occurred with the generation of the crack at the section A-A' at a specific angle during the 2nd sequence by the knockout pin. Because the profile of the cross section varies according to the critical damage value in the analysis of the trimming process, it is very important to acquire accurate material properties and critical damage values throughout each experiment. The sheared plane profile and FE-analysis results of the optimized process are presented in Fig. 27 and Table 13. Consequently, the sound shear surface and the minimum trimming load were obtained, compared with the FE-analysis results presented in the orthogonal array table.

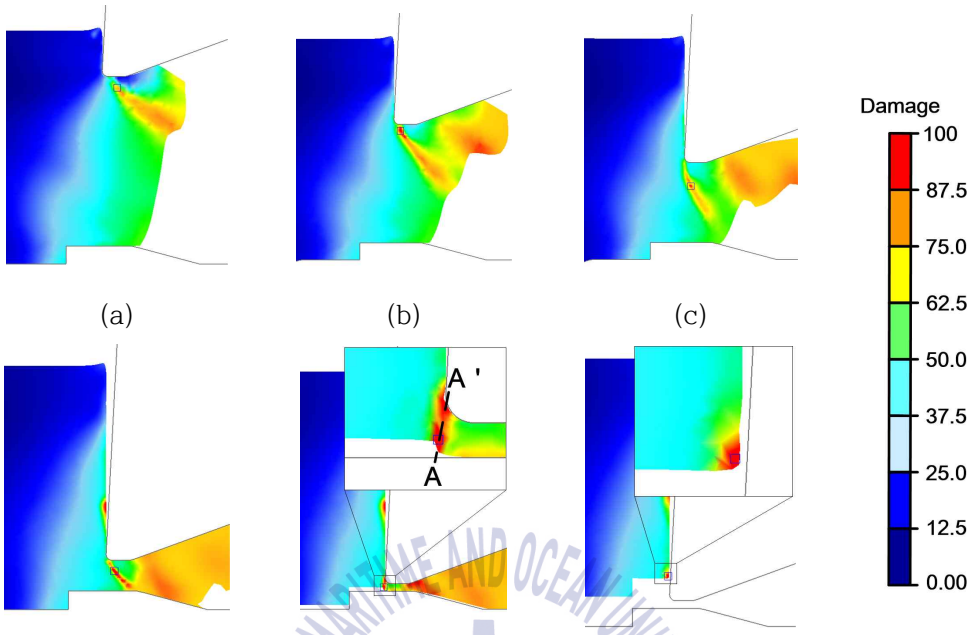

Fig. 25 Damage distribution of optimum process condition: (a) 19.9% stroke (b) 40.4% stroke (C) 60.9% stroke (d) 88.7% stroke (e) Shear by knockout pin (f) Final state

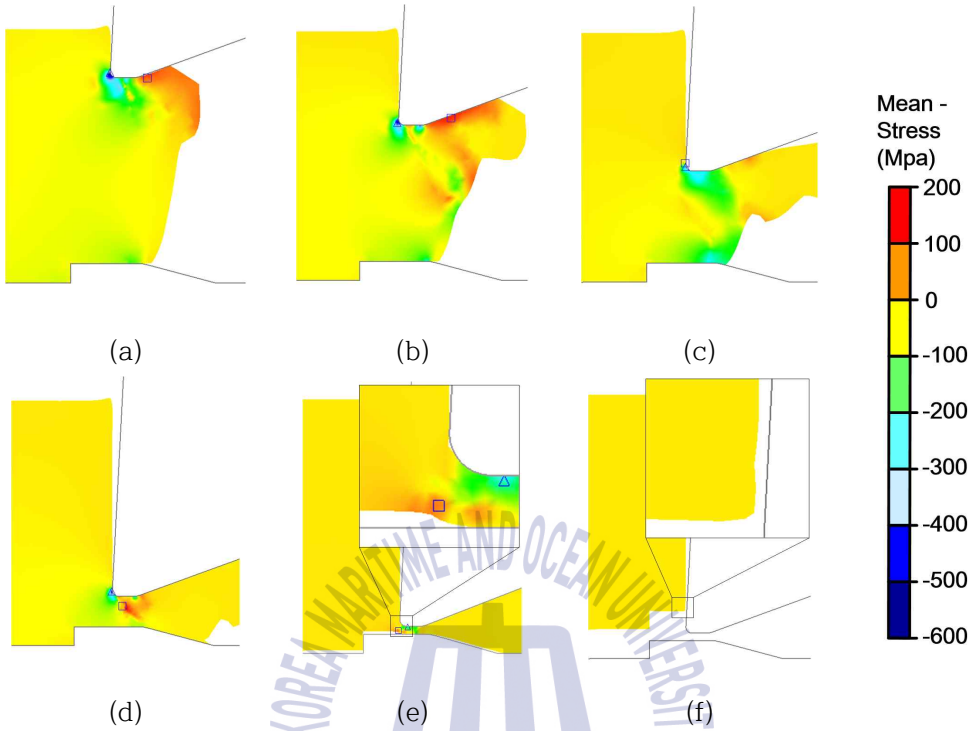

Fig. 26 Mean stress distribution of optimum process condition: (a) 19.9% stroke (b) 40.4% stroke (C) 60.9% stroke (d) 88.7% stroke (e) Shear by knockout pin (f) Final state

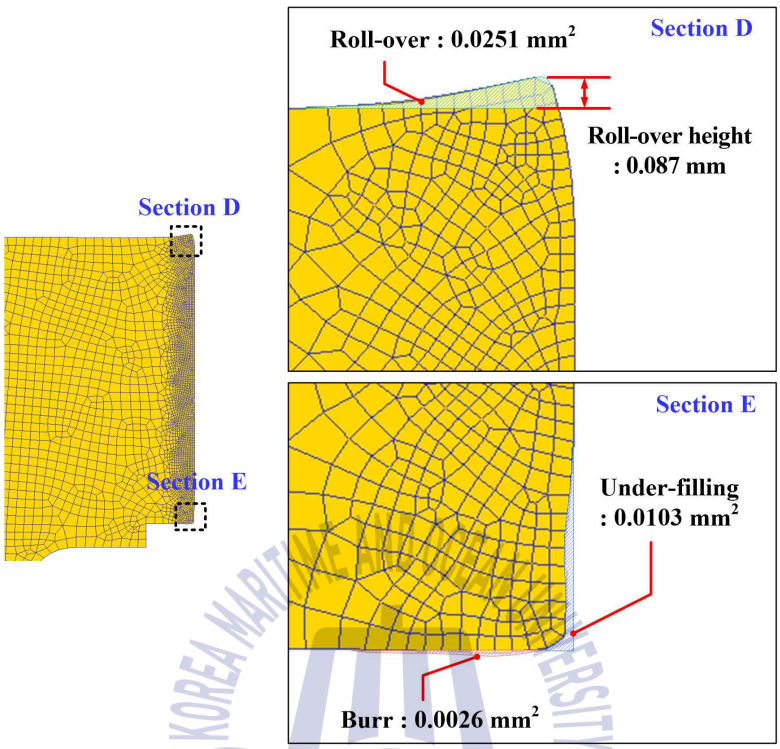

Fig. 27 FE-analysis results for the profile of shear surface

Table 13 FE-analysis results of the optimized trimming process

Objective functions	Values	
Shape defects (mm^2)	Roll-over	0.0251
	Under-filling	0.0103
	Burr	0.0026
	Total	0.038
Peak trimming load (N)	42,414	

However, as shown in Fig. 28, roll-over occurred owing to the indentation of the punch at the upper part of the bolt head. Generally, the roll-over during the sheet shearing process is generated toward the direction of the punch stroke owing to the bending moment. However, because of the reaction force from the bottom die, the material near the blade edge at the head upper section bulges up as much as the volume of the punch's penetration in the bolt-trimming process. As the BR of the punch increases, the roll-over becomes larger. Therefore, it is preferable that the BR be designed to be as small as possible.

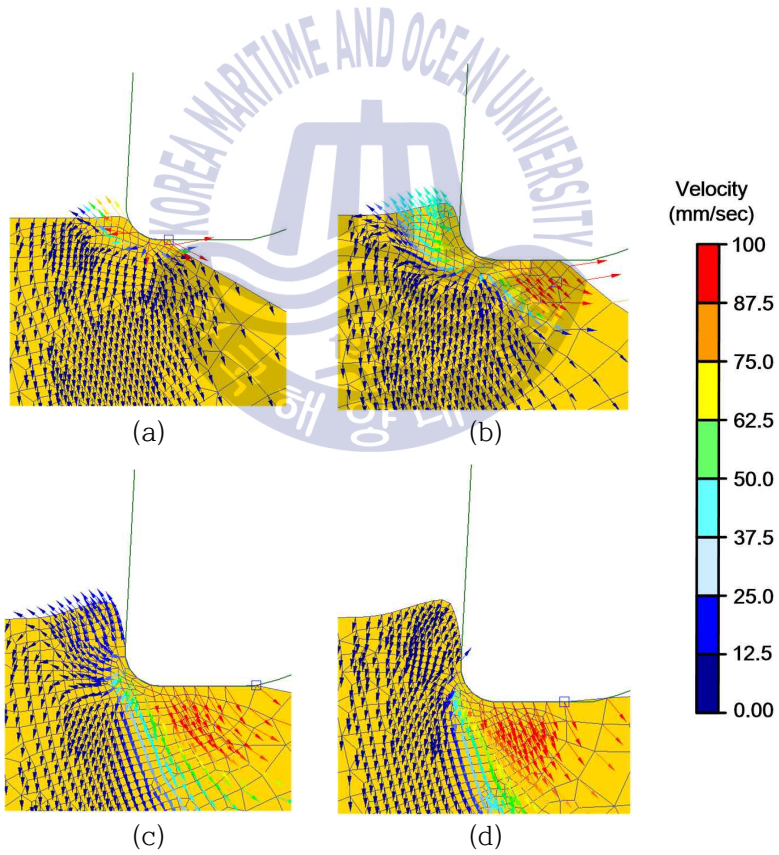

Fig. 28 Velocity distribution on upper part of bolt head: (a) 0.025% stroke (b) 0.15% stroke (C) 0.3% stroke (d) 0.45% stroke

4. FE-analysis of thread-rolling process

4.1 Design of experiment for thread-rolling process

Based on the theoretical design results, we optimized the thread-rolling process of Al6061 alloy bolts using the Taguchi method. To do this, three design parameters (See Fig. 5 and Fig. 30) and two objective functions (See Fig. 29) are specified. In addition to the PD defined at theoretical design step, transfer velocity (TRV) and revolutions per minute (RPM) are were chosen as design parameters, which are mainly considered in the actual industrial field. The ranges of TRV and RPM are determined based on the operating condition of the manufacturing sites. The levels of design parameters are set as shown in Table 14. Further, the $L_9(3^3)$ orthogonal array table for the application of the Taguchi method and FE-analysis is displayed in Table 15.

Table 14 Design parameters and their levels for thread-rolling process

Parameters	Level 1	Level 2	Level 3
Penetration depth (PD) [mm]	0.2	0.3	0.4
Transfer velocity (TRV) [mm/s]	0.5	1.0	1.5
Revolution per minute (RPM) [rev/min]	0.25	0.5	0.75

Table 15 $L_9(3^3)$ orthogonal array table for thread-rolling

No. of simulation	PD	TRV	RPM
1	1.08	1.6	12
2	1.08	2	15
3	1.08	2.4	18
4	1.135	1.6	15
5	1.135	2	18
6	1.135	2.4	12
7	1.19	1.6	18
8	1.19	2	12
9	1.19	2.4	15

One of the objective functions is the mean under-filling rate (UR_{mean}) of the formed thread to evaluate the dimensional accuracy, and is defined as Eq. (28):

$$UR_{mean} = \left[\sum_{i=1}^{N}\left(\frac{A_{i,die} - A_{i,thread}}{A_{i,die}}\right)\times 100\right]/N \tag{28}$$

where $A_{i,die}$ is the cross-sectional area of the thread profile of the position i for the thread-rolling dies, $A_{i,thread}$ is the cross-sectional area of the thread profile of the position i for the bolt thread, and N is the number of sampled threads.

The other objective function is the maximum thread-rolling load (*Max. load*), which influences the life cycle of the thread-rolling dies. As shown in Fig. 29, the maximum load is observed at the completion step of the penetration, and afterward, only the rotation process continues. Because the values of UR_{mean} and *Max. load* were intended to be a minimum in the thread-rolling process, the-smaller-the-better characteristics, such as the trimming process, was applied to calculate the SN ratio.

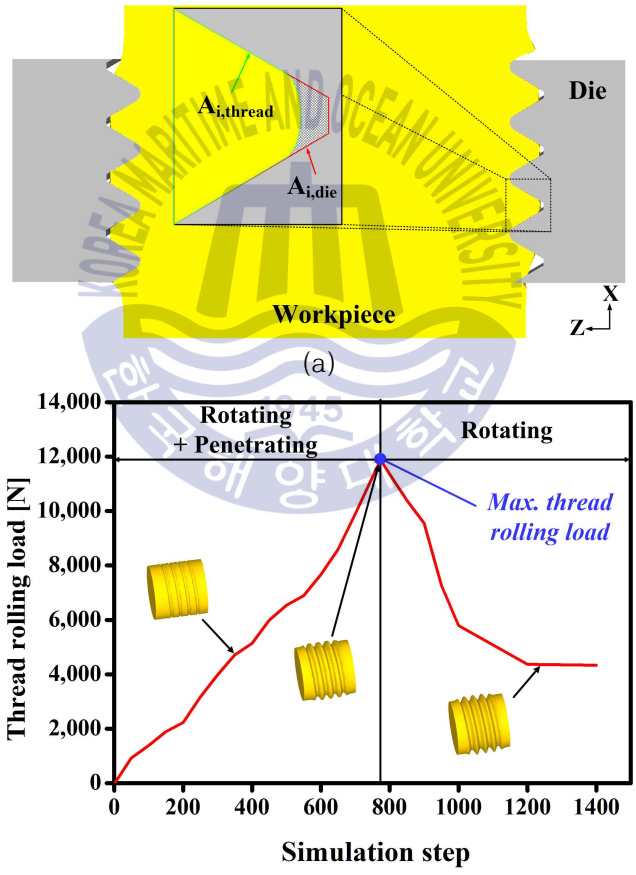

Fig. 29 Descriptions of objective functions: (a) UR_{mean}, (b) *Max. load*

4.2 Conditions of FE-analysis in thread-rolling process

Based on the DOE using the Taguchi method, the FE-analysis for the thread-rolling process was carried out using the DEFORM-3D software. According to the preceding study[23], three-dimensional (3D) FE-analysis is necessary to consider the effects of the groove orientation and the movement of the workpiece. The 3D FE-model has the following features:

(1) Thread-rolling dies are set as rigid bodies. The TRV is applied in the directions of the moving die and the stationary die to indent the workpiece. To prevent the workpiece from escaping from the dies, the center axis of the workpiece is fixed, allowing it to rotate only.

(2) The 3D tetrahedral elements in the workpiece are used, and a finer mesh is applied in the deformation zone to ensure convergence and accuracy of the simulation. Considering the computational time, the number of teeth is set to be four. As a result, the number of elements and nodes is 128,836 and 28,593, respectively.

(3) In general, conventional liquid lubricants, adhering to the dies and the workpiece, are hindered from reaching the contact area during thread-rolling because they are pressed out of the contact area[31]. Therefore the friction factor (m) is set to 0.9, which is nearly the dry friction state, in order to suppress the sliding between the dies and the workpiece[27].

Fig. 30 and Fig. 31 demonstrate the 3D FE-model of the thread-rolling process and the stress-strain curve of Al6061-T6, respectively.

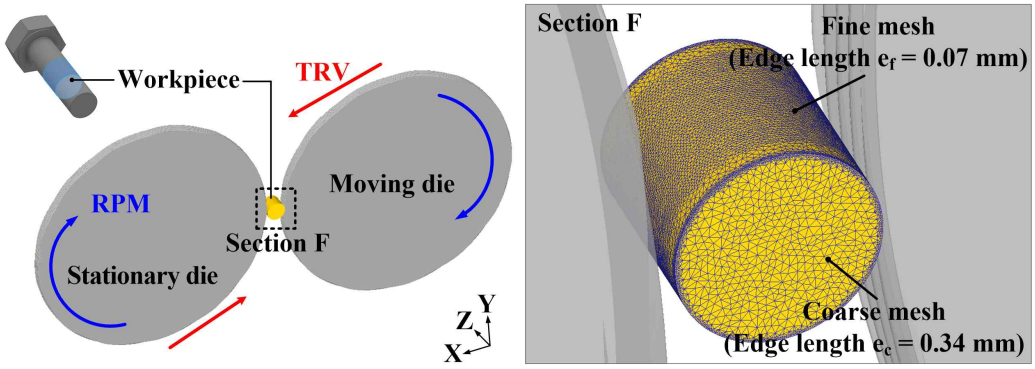

Fig. 30 3D FE-model of the thread-rolling process

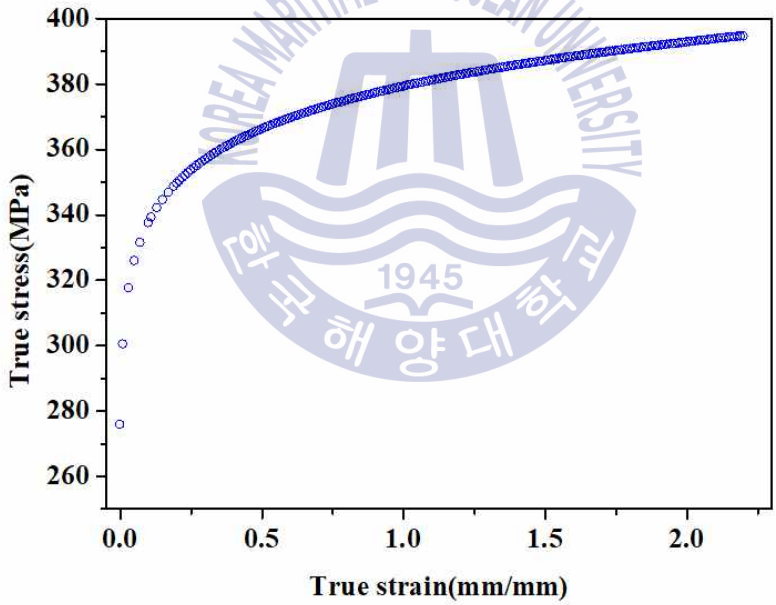

Fig. 31 Stress-strain curve of Al6061-T6

4.3 Results of FE-analysis in thread-rolling process

Table 16 and Table 17 show the results of the FE-analysis and the Taguchi method for the UR_{mean} and *Max. load*, respectively. From the ANOVA results, it was revealed that among the design parameters, PD has the most significant contribution on UR_{mean} and *Max. load* by 96.9% and 78.8%, respectively. In case of the UR_{mean}, the influence of the TRV and the RPM is somewhat small, but the TRV has a slightly higher influence than the RPM. Meanwhile, for Max. load, the effect of RPM was slightly higher than that of the TRV. The results of analysis of variance are given in Table 18 and Table 19.

Based on the calculations for the mean SN ratios, the main effect plots of factors with respect to objective functions are drawn in Fig. 32. The combination of design parameters that maximizes the SN ratio for UR_{mean} was set as: PD 1.19 mm, TRV 1.6 mm/s, and RPM 18 rev/min, and in the case of *Max. load*, PD 1.08 mm, TRV 1.6 mm/s, and RPM 18 rev/min.

Most analysis results showed the tendency for UR_{mean} to decrease by 70–90% and for *Max. load* to increase by 5–20% when PD increases by 0.055 mm. However, it is interesting to note that the highest value of *Max. load* was found in the 6^{th} simulation. Also, a relatively high UR_{mean} appeared under the same PD condition. The above results indicate that the PD is the most influential process parameter, but an additional consideration is needed on the influence of other design parameters. Therefore, to identify the influence of other parameters clearly, i.e., TRV and RPM, the transfer per revolution (*TPR*), which combines TRV and RPM, was newly applied to indicate the amount of penetration per unit revolution by the thread-rolling dies, as shown in Eq. (29):

$$TPR = \frac{TRV}{RPM} \times 60 \tag{29}$$

It is can be seen that UR_{mean} and *Max. load* tend to be very similar on the same PD level depending on the variation of *TPR*, as indicated in Fig. 33. At the same time, with the increase in PD, UR_{mean} decreased and *Max. load* increased generally. However, as mentioned above, the results of the 6th and 7th simulation were different from this tendency. When it comes to the simulation no. 6, the PD is the level of 2 (1.135 mm), but the *TPR* is 12 mm/rev, which is the highest among all the simulations. At this time, the *Max. load* occurred and the UR_{mean} was relatively higher than other simulation results of the same PD condition. On the contrary, in case of the simulation no. 7, the *TPR* is minimum (5.3 mm/rev) and the *Max. load* showed the lowest value among the results of simulations of the same PD level.

To analyze this phenomenon, the contact area between the workpiece and dies, as well as the radial velocity of the workpiece were investigated for case A (i.e., simulation no. 6) and case B (i.e., simulation no. 7) with the maximum and minimum values of *TPR* being 12 mm/rev and 5.3 mm/rev, respectively.

Table 16 Results of FE-analysis for UR_{mean}

No. of simulation	UR_{mean} [%]	SN ratio
1	4.833	-13.6843
2	5.021	-14.0158
3	5.016	-14.0072
4	0.495	6.1079
5	0.500	6.0206
6	1.244	-1.8964
7	0.103	19.7433
8	0.161	15.8635
9	0.151	16.4205

Table 17 Results of FE-analysis for *Max. load*

No. of simulation	*Max. load* [N]	SN ratio
1	6,930	-76.8147
2	6,810	-76.6629
3	6,830	-76.6884
4	7,230	-77.1876
5	7,300	-77.2688
6	8,920	-79.0073
7	8,520	-78.6088
8	8,790	-78.8798
9	8,770	-78.8600

Table 18 Results of analysis of variance for UR_{mean}

Parameter	SS	DOF	V	P [%]
PD	1470.0	2	735.0	96.9
TRV	23.13	2	11.56	1.52
RPM	23.32	2	11.66	1.53

Table 19 Results of analysis of variance for *Max. load*

Parameter	SS	DOF	V	P [%]
PD	6.38	2	3.19	78.8
TRV	0.762	2	0.38	9.42
RPM	0.949	2	0.47	11.7

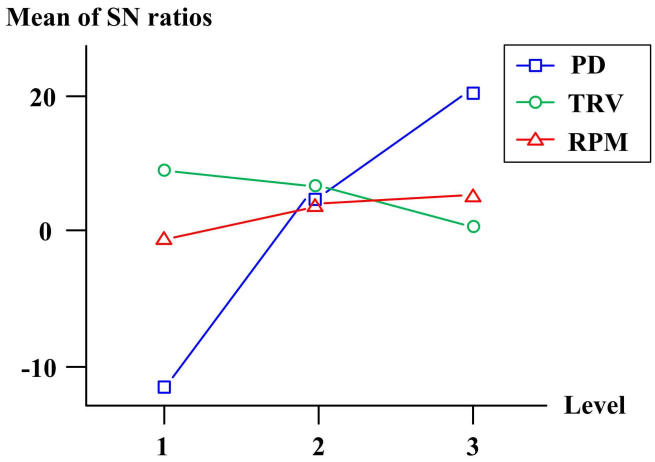

(a)

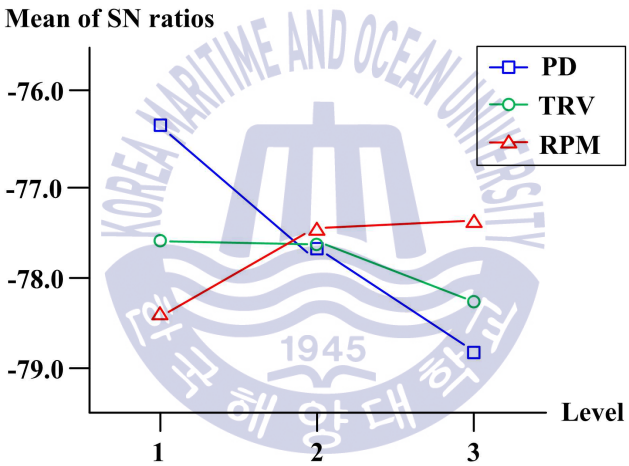

(b)

Fig. 32 Main effect plots on objective functions in thread-rolling process: (a) UR_{mean}, (b) *Max. load*

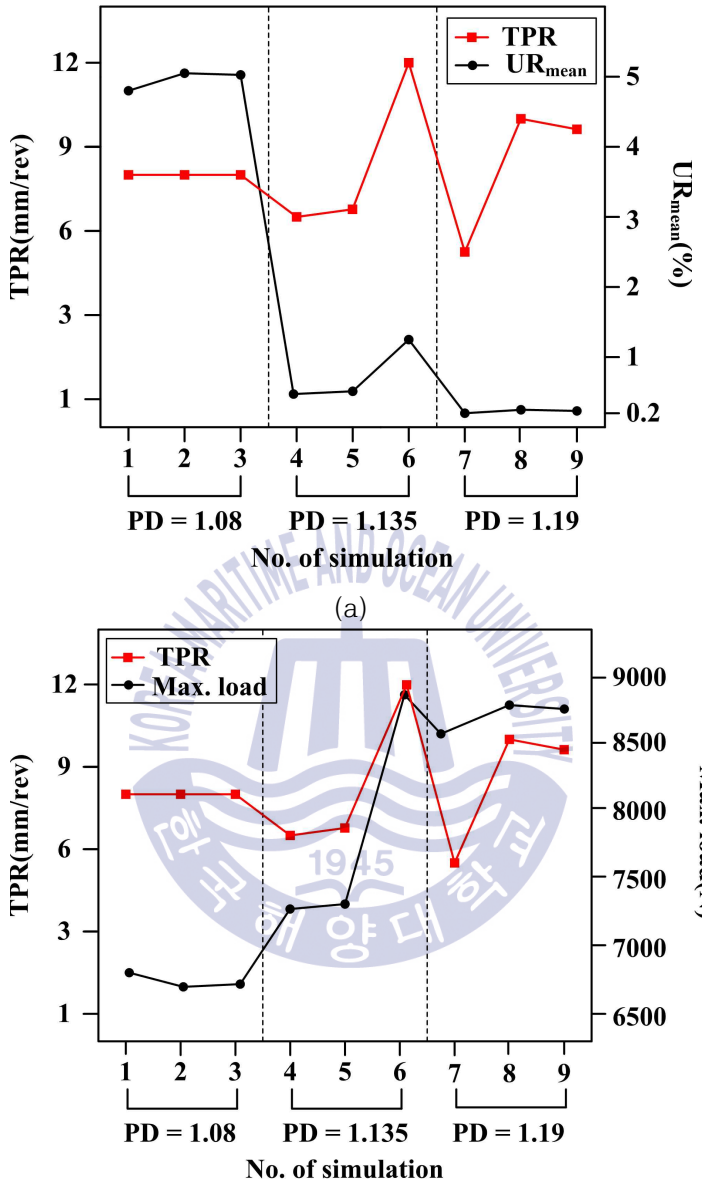

Fig. 33 FE-analysis results depending on *TPR*: (a) UR_{mean}, (b) *Max. load*

The contact area between the workpiece and the dies during the FE-analysis of case A and case B under the same indentation level (PD = 1.0)

is illustrated in Fig. 34. In the analysis result of the larger *TPR* (case A), the material and dies make contact in the more extensive area compared with the case B. A larger contact area means that a higher forming load is required. Furthermore, as shown in Fig. 35, there is a significant difference in the radial velocity distribution of the material in the deformation zone during the process. The velocity field of case B in the deformation zone with a relatively smaller value of *TPR* shows a higher mean value than that of the analysis result for case A. This indicates that there is a smoother flow of material during the process, resulting in sound filling of the material. Therefore, it can be seen that the lower the value of the *TPR* that is set, the lower is the under-filling ratio and the forming load that can be achieved in the thread-rolling process, progressive forming through the rotation and transfer movement by rolling dies.

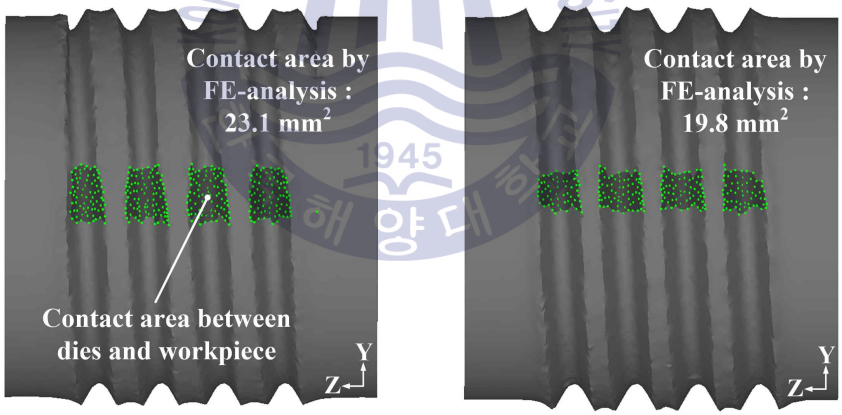

(a) (b)

Fig. 34 Comparison of contact area between the workpiece and the dies during the FE analyses of case A and case B under the same penetration level (PD = 1.0 mm).

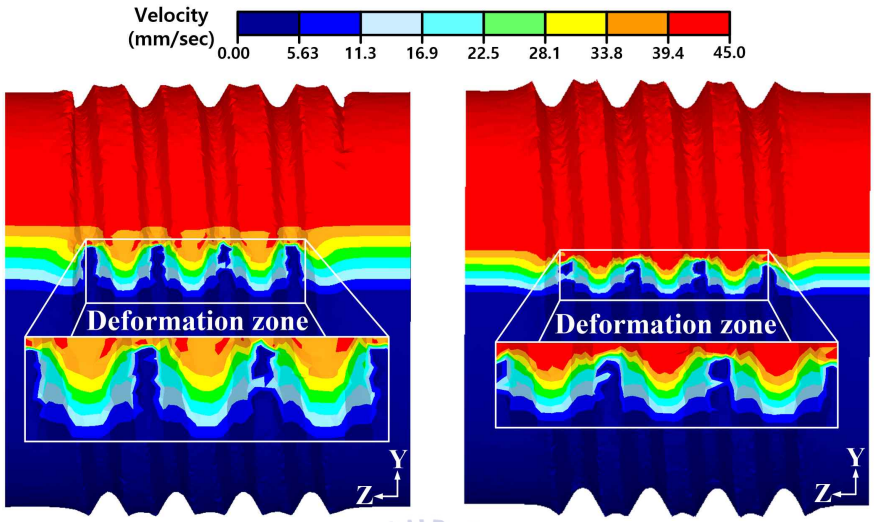

(a) (b)

Fig. 35 Comparison of the radial velocity distribution of the material in the deformation zone during the process (PD = 1.0 mm).

From the above results, the optimal process conditions were derived considering the PD and *TPR*. However, with respect to PD, UR_{mean} and *Max. load* tend to be opposite to each other. When the variation range of the SN ratio is compared, the influence of PD on UR_{mean} is larger than that on *Max. load*. It is also important that the threads should be completely formed so that the dimensions of the formed threads meet the standard requirements. Therefore, PD is determined based on UR_{mean}, and the TRV and RPM values are set to be the lowest value of *TPR*. The optimum process conditions obtained by the Taguchi method and FE-analysis are set as: PD = 1.19 mm, TRV = 1.6 mm/s, and RPM = 18 rev/min.

By applying the optimum process conditions in the FE-analysis, the lowest thread-rolling load (8520 N) and the least under-filling rate (0.103%) were acquired compared with the results of the FE-analysis using the orthogonal array table. The thread profile and effective strain distribution according to

the number of revolutions of the thread-rolling process are displayed in Fig. 36. It is confirmed that the analytical model shows the same tendency as the industrial practices, considering that the thread was completely developed within five to six revolutions. Until the 4th rev, the dies simultaneously press the material and form the thread gradually. After the indentation is completed, the process is conducted by only the rotation of dies. Fig. 37 shows the effective strain distribution on the cross-section of the deformed thread when the thread-rolling process is completed. The strain is increasing toward the peak of the thread, and shows the maximum effective strain of 4.77 in the peak and the minimum effective strain of 3.95 in the root. Furthermore, it is shown that the incremental forming process is conducted, showing the uniform strain distribution along the bolt-axis direction.

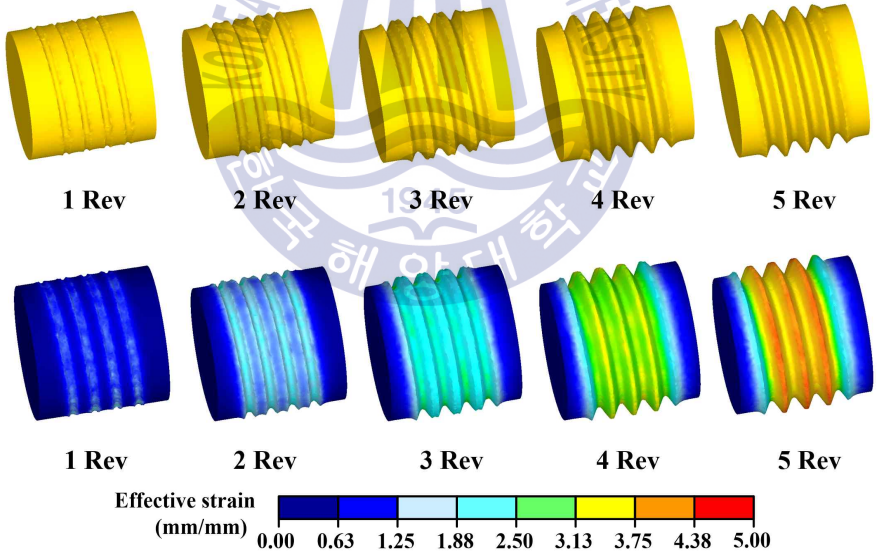

Fig. 36 Thread profile and effective strain distribution according to the number of revolutions of the thread-rolling process.

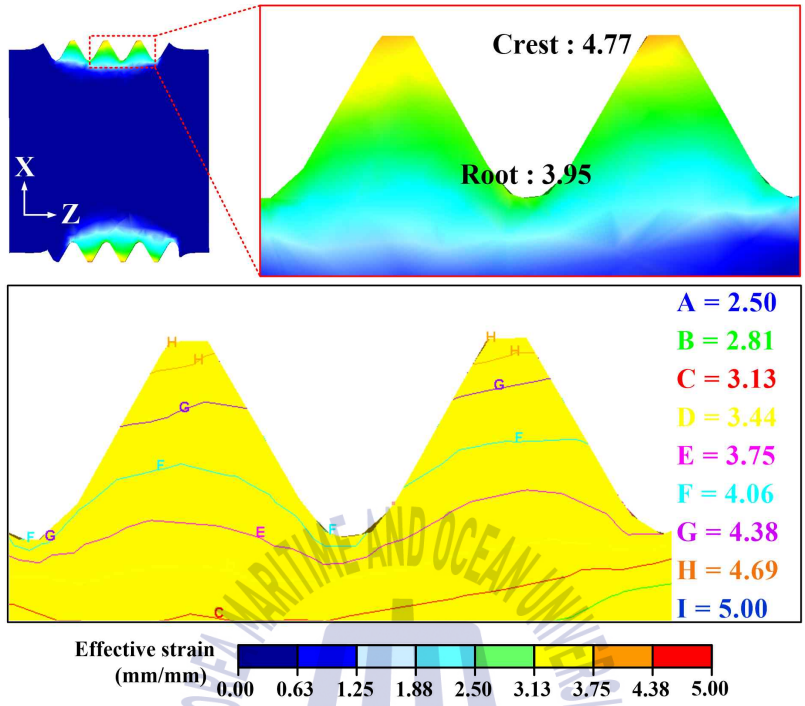

Fig. 37 Effective strain distribution on the cross-section of the deformed thread.

5. Experiment for manufacturing Al6061 alloy bolts

5.1 Experimental procedure

In order to experimentally verify the validity of the proposed design method for the integrated forming process, several bolt manufacturing experiments have been carried out using Al6061 alloy. The cold-former and thread-rolling machine, which are used in this work with a maximum forming force of around 400 tons and 30 tons, respectively, are shown in Fig. 38. The experimental conditions are the same as those determined from the theoretical design and FE-analysis stage, and are as follows:

(1) The initial material used for cold-former forging is Al6061 alloy with a diameter and length of Ø10.58 mm and 75 mm, respectively, and is annealed in a furnace to improve the formability.

(2) The products of the cold-former forging process are delivered to the thread-rolling machine after T6 heat treatment to eliminate the residual stress and improve the mechanical properties.

(3) The trimming and thread-rolling process are carried out on the optimum condition derived from the Taguchi method, i.e., BR = 0.2 mm, LW = 1.0 mm, and SD = 0.25 mm for the trimming process, and PD = 1.19 mm, TRV = 1.6 mm/s, and RPM = 18 rev/min for the thread-rolling process, respectively.

(4) The lubricating oils are Wellformer 600 for cold-former forging and thread-rolling lubricants of ISO VG grade 10 used in manufacturing sites.

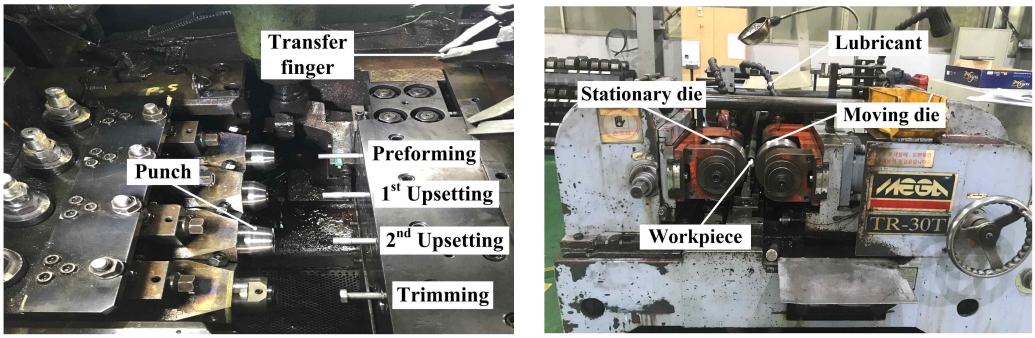

(a) (b)

Fig. 38 Experiment equipment for manufacturing Al6061 alloy bolts: (a) cold-former, (b) thread-rolling machine.

5.2 Experimental results

Fig. 39 displays the produced Al6061 alloy bolt shape at each stage of the integrated forming process. First, the application of process limitations to prevent cracks and buckling in the heading process as well as the design of the preform considering the metal flow were verified, resulting in the sound shape of the bolt head. We also found that the point with the highest damage value of 66.7 (See Fig. 15(b)) showed no defects, and the shear-section profile of the trimmed bolt head is in good agreement with that obtained from the FE-analysis, as presented in Fig. 40. Thus, it was proven that FE-analysis based on the ductile fracture criterion was effective. Besides, as shown in Fig. 41 and Table 20, the dimension of the deformed thread part is very similar to the design shape. Consequently, the design method for the integrated forming process of aluminum alloy bolts led to the successful product shape without any defect and the highest dimensional accuracy.

Fig. 39 Produced Al6061 alloy bolt shape at each stage

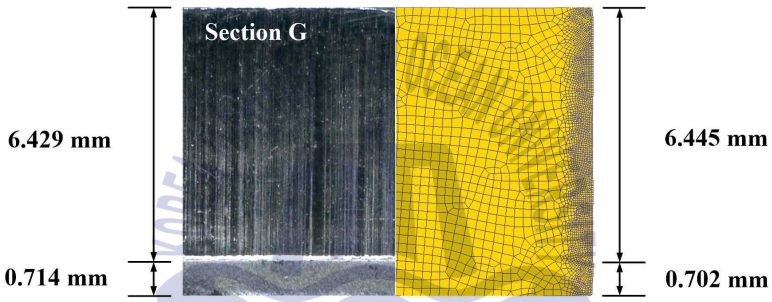

Fig. 40 Comparison of shear section with FE-analysis result

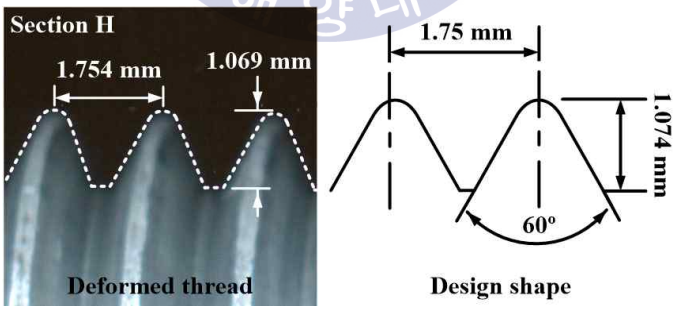

Fig. 41 Comparison of deformed thread section with design shape

Table 20. Comparison of FE-analysis and experiment for the thread major diameter

(unit: mm)

Design standard	FE-analysis	Experiment
11.708	11.711	11.71

6. Conclusions

In this study, we proposed an integrated manufacturing process design method for Al6061 alloy bolts to fasten marine structures, and the following conclusions were made.

(1) The theoretical design was performed as a preliminary design phase to manufacture Al6061 alloy bolts. In the thread-rolling process, the initial rod diameter and the PD range of the rolling dies was set using Eq. (1) and Eq. (2), respectively. By applying the volume constancy law, process limitations for defect predictions (Eqs. (3)-(4)), and K. Lange's design rule, the dimensions of the workpiece, number of stages, and preform for the heading process were determined, respectively. The forging force in the heading was also predicted by the slab method to evaluate the process feasibility.

(2) We conducted a numerical study to validate the theoretical design of the heading and thread-rolling process, and to optimize the trimming and thread-rolling processes. The results of the FE-analysis in the heading process indicated that the maximum damage value of 66.7 was lower than the critical damage value of 74.4 obtained by Cockcroft & Latham's ductile fracture criterion. Thus, it was considered that the heading process could proceed without any defect. The maximum forming load estimated by FE analysis for the heading was 13.9 tons in the 2^{nd} upsetting process, which was feasible value, considering the capacity of cold-former for the forming experiment (400 tons). Furthermore, by comparing the results with ones by the slab method, the theoretical model using the slab method was proven to be effective.

(3) The results of the FE-analysis based on Taguchi method revealed that BR had the greatest effect on the shape defects and forming load during the

trimming process. In the thread-rolling process, PD was the design parameter which played a key role in the under-filling rate and forming load. However, it was noticeable that *TPR*, which is the amount of penetration per unit revolution by the thread-rolling dies, was also a vital factor, resulting in a smoother metal flow and lower forming load.

(4) By performing the bolt-forming experiment using Al6061 alloy, the proposed design method was evaluated in terms of the shape and dimensional accuracy. As a result, a successful bolt shape without defects was obtained, resulting in a clear sheared plane of the bolt head in good agreement with FE-analysis. In addition, the deformed thread section showed a high level of dimensional precision compared to the design standard and FE-analysis result. Thus, it can be concluded that the design method proposed in this study could be widely applied to design the integrated manufacturing process for various sizes of bolts in industrial fields.

References

[1] Jürgen, H., 2014. Recent development in aluminium for automotive applications. *Transactions of Nonferrous Metals Society of China*, 24, pp.1995-2002.

[2] Kim, S.J., Jang, S.K., Han, M.S., Park, J.C., Jeong, J.Y., & Chong, S.O., 2013. Mechanical and electrochemical characteristics in sea water of 5052-O aluminum alloy for ship. *Transactions of Nonferrous Metals Society of China, 23,* pp.636-641.

[3] Chiu, L.H., Tsai, C.Y., Chen, K.H., Hu, C.J., & Chang, H., 2015. Effect of coarse second-phase particles on galvanic corrosion of anodized 6061 aluminum alloy coupled with c1100 copper. *International Journal of Electrochemical Science*, 10, pp.6572-6585.

[4] Shin, Y.W. & Kawai, K.I., 1991. A study of optimum die design in the heading process with two blows_part1: Experimental study. *Journal of Materials Processing Technology, 28,* pp.391-406.

[5] Yoon, D.J., Hahm, S.Y., & Lee, Y.S., 2012. A study on forming of Al-Zn-Mg-Sc aluminum alloy bolts. *Transactions of Materials Processing*, 21(7), pp.447-452.

[6] Kim, J.W., Chae, S.W., Han, S.S., & Son, Y.H., 2010. Manufacturing process design of aluminum alloy bolt. *Journal of the Korean Society for Precision Engineering*, 27(5), pp.63-68.

[7] Choi, J.S., Nawaz, S., Hwang, S.K., Lee, H.C., & Im, Y.T., 2010. Forgeability of ultra-fine grained aluminum alloy for bolt forming. *International Journal of Mechanical Sciences*, 52, pp.1269-1276.

[8] Jin, Y.G., Baek, H.M., Hwang, S.K., Im, Y.T., & Jeon, B.C., 2012. Continuous high strength aluminum bolt manufacturing by the spring-loaded ECAP system. *Journal of Materials Processing Technology*, 212, pp.848-855.

[9] Kim, J.H., Hwang, S.K., Im, Y.T., Son, I.H., & Bae, C.M., 2012. High-strength bolt-forming of fine-grained aluminum alloy 6061 with a continuous hybrid process. *Materials Science and Engineering*, A(552), pp.316-322.

[10] Choi, H.S., Kim, S.G., Choi, H.K., Kim, B.M., & Ko, D.C., 2012. The effect of clearance and inclined angle on sheared edge in trimming of UHSS. *Proceedings of the Korean Society for Technology of Plasticity fall conference*, pp.440-443.

[11] Lee, J.H., Lee, K.H., & Lee, S.B., 2016. Process design of trimming to improve the sheared-edge of the vehicle door latch based on the FE simulation and the Taguchi method. *Journal of the Korea Academia- Industrial Cooperation Society*, 117(11), pp.483-490.

[12] Li, M., 2000. An experimental investigation on cut surface and burr in trimming aluminum autobody sheet. *International Journal of Mechanical Sciences*, 42, pp.889-906.

[13] Han, X., Yang, K., Ding, Y., Tan, S., & Chen, J., 2016. Numerical and experimental investigations on mechanical trimming process for hot stamped ultra-high strength parts. *Journal of Materials Processing Technology*, 234, pp.158-168.

[14] MacCormack, C. & Monaghan, J., 2001. A finite element analysis of cold-forging dies using two- and three-dimensional models. *Journal of Materials Processing Technology*, 118, pp.286-292.

[15] MacCormack, C. & Monaghan, J., 2001. Failure analysis of cold forging dies using FEA. *Journal of Materials Processing Technology*, 117, pp.209-215.

[16] Kim, K.W., Lee, G.T. & Cho, H.Y., 2016. A forging die design to improve the flower shape of flange bolt. *Journal of the Korean Society of Marine Engineering*, 40(4), pp.314-319.

[17] Kim, K.W., Qiu, Y.G. & Cho, H.Y., 2016. Design of eccentric forging process for camber bolts using finite element method. *Journal of the Korean Society of Marine Engineering*, 40(4), pp.320-324.

[18] Kim, K.W., Kim, Y.T., Kim, W.J. & Cho, H.Y., 2008. Finite element analysis for multi-stage forging process design of bolt with nonaxisymmetric washer cam. *Journal of the Korean Society of Marine Engineering*, 32(4), pp.585-595.

[19] Park, S.C. & Lee, K.H., 2018. Design of the trimming process of an Al6061 alloy bolt head using finite element analysis and the taguchi method. *Journal of the Korean Society of Marine Engineering*, 42(10), pp.800-806.

[20] Amstead, B.H., Phillip, F.O. & Myron, L.B., 1987. *Manufacturing Processes*. 8th Ed. Wiley.

[21] Lee, J.E., Kim, J.B. & Park, G., 2017. An Investigation of thread-rolling characteristics of titanium micro-screws according to die design parameters. *Journal of the Korean Society of Precision Engineering*, 34(2), pp.88-93.

[22] Lee, J.E., Kim, J.B., Park, G. & Ra, S.W., 2016. Investigation into thread-rolling characteristics of subminiature screws according to thread shapes. *Transactions of the Korean Society of Mechanical Engineers-A*, 40(11), pp.971-978.

[23] Domblesky, J.P. & Feng, F., 2002. Two-dimensional and three-dimensional finite element models of external thread-rolling, *Proceedings of the Institute of Mechanical Engineers, Part B: Journal of Engineering Manufacture*, 216(4), pp.507-517.

[24] Domblesky, J.P. & Feng, F., 2002. A parametric study of process parameters in external thread-rolling, *Journal of Materials Processing Technology*, 121(2-3), pp.341-349.

[25] Hsia, S.Y., Pan, S.K. & Chou, Y.T., 2015. Computer simulation for flat-die thread-rolling of screw, *International Conference on Innovation, Communication and Engineering*.

[26] Kim, K.H., Kim, D.H., Ko, D.C. & Kim, B.M., 2002. Characteristics evaluation of process parameters for improvement the precision of thread-rolling in lead screw, *Annuals Autumn Conference of Korean Society of Precision Engineering*, pp.312-315.

[27] Kim, K.H., Kim, D.H., & Kim, B.M., 2002. Determination of optimal blank diameter for the high precision of spindle screw, *Transaction of Materials Processing*, 11(8), pp.170-175.

[28] Song, J.H., Lee, J.S., Lee, H.J., Lee, G.A., Park, K.D, Ra, S.W. & Lee, H.W., 2011. Analysis and experiments on the thread-rolling process for micro-sized screws – Part 1

: Process parameter analysis by finite-element simulation, *Transaction of Materials Processing,* 20(8), pp.581-587.

[29] Song, J.H., Lee, J.S., Lee, H.J., Lee, G.A., Park, K.D, Ra, S.W. & Lee, H.W., 2012. Numerical analysis and experimental study of thread-rolling process for micro-sized screws – Part 2 : Application to a micro-screw with diameter of 800μm, *Transaction of Materials Processing,* 21(3), pp.179-185.

[30] Shin, M.S., Cha, S.H., Kim, K.B., Kim, J.H. & Ra, S.W., 2009. Lead screw process design by thread-rolling analysis, *Annuals Spring Conference of The Korean Society of Mechanical Engineers,* pp.1312-1316.

[31] Kramer, P. & Groche, P., 2018. Defect detection in thread-rolling processes – Experimental study and numerical investigation of driving parameters, *International Journal of Machine Tools and Manufacturing,* 129, pp.27-36.

[32] Park, S.C., Dong, W.R. & Lee, K.H., 2018. Design of a thread-rolling process for manufacturing Al6061-T6 alloy bolt using FE-analysis and the Taguchi method, *Journal of the Korean Society of Marine Engineering,* 42(6), pp.443-450.

[33] Edwards, G.A., Stiller, K., Dunlop, G.L. & Couper, M.J., 1998. The precipitation sequence in Al-Mg-Si alloys, *Acta Materialia.* 46(11), pp.3893-3904.

[34] Jensrud, O. & Pedersen, K., 1998. Cold forging of high strength aluminum alloys and the development of new thermomechanical processing. *Journal of Materials Processing Technology,* 80-81, pp.156-160.

[35] Altan, T., Ngaile, G. & Shen, G., 2005. *Cold and Hot Forging Fundamentals and Application.* ASM International.

[36] Chen, S., Qin, Y., Chen, J.G. & Choy, C.M., 2018. A forging method for reducing process steps in the forming of automotive fasteners. *International Journal of Mechanical Sciences,* 137, pp.1-14.

[37] Feng, W. & Hua, L., 2011. Multi-objective optimization of process parameters for the helical gear precision forging by using Taguchi method. *International Journal of Mechanical Sciences,* 25(6), pp.1519-1527.

[38] ASM Handbook Committee, 1991. *ASM Handbook, Volume 4: Heat Treating*. 10th Ed. ASM International.

[39] ASME, 2005. *Metric Screw Threads: M profile (B1.13M-2005)*. ASME.

[40] ASME, 2005. *Metric Formed Hex Screws (B18.2.3.2M-2005)*. ASME.

[41] Gokler, M.I., Dean, T.A. & Knight, W.A., 1982. Computer-aided sequence design for hot upset forgings. *Proceedings of the Twenty-second International Machine Tool Design and Research Conference*, pp.457-466.

[42] Heinz, T., 2006. *Metal forming practise : processes - machines – tools*. Springer-Verlag Berlin Heidelberg.

[43] Lange, K., 1995. *Handbook of metal forming*. Society of Manufacturing Engineers.

[44] Altan, T., Oh, S.I. & Gegel, H.L., 1983. *Metal forming: fundamentals and applications*, American society for metals.

[45] O'Connell, M., Painter B., Maul, G. & Altan, T., 1996. Flashless closed-die upset forging-load estimation for optimal cold header selection. *Journal of Materials Processing Technology*, 59, pp.81-94.

[46] Kim, H.S., Im, Y.T. & Geiger, M., 1999. Prediction of ductile fracture in cold forging of aluminum alloy. *Journal of Manufacturing Science and Engineering*, 121, pp.336-344.

[47] Petruska, J., Borkovec, J., Hulka, J. & Foret, R., 2011. Application of ductile fracture criteria to industrial cutting processes. *Advanced Materials Research*, 264-265, pp.913-918.

감사의 글

석사과정을 마치면서 지난 2년간의 대학원 생활을 돌이켜보면 학문적으로, 그리고 경험적으로도 많은 것을 배울 수 있었던 귀중한 시간이었습니다. 많은 분들의 관심과 격려 덕분에 이렇게 학위논문을 내기까지 행복했던 대학원 생활을 보낼 수 있었습니다.

먼저 부족한 저를 제자로 받아 주시고 따뜻한 관심과 세심한 지도로 참된 가르침을 베풀어 주신 이경훈 교수님께 고개 숙여 감사의 마음을 전하고 싶습니다. 지도 교수님으로서, 그리고 인생의 선배로서 저에게 해주신 진심 어린 조언들을 항상 가슴에 새기고 절실한 마음으로 연구에 몰두할 수 있는 공학도로 성장해 나가겠습니다. 또한, 고민과 선택의 기로마다 깊은 혜안으로 저를 이끌어 주신 김명환 교수님께도 진심으로 감사의 말씀을 드립니다. 그리고 바쁘신 가운데 논문을 심사해 주시고 학문적으로도 많은 가르침을 베풀어 주신 심도식 교수님께도 감사를 드리며, 기계융합·재료공학 전공을 공부하면서 학문의 큰 숲을 바라볼 수 있게 지도해 주시고 많은 조언을 해주신 이명훈 교수님, 연구자로서 연구에 임하는 자세를 깨우쳐 주신 김종도 교수님께 깊은 감사의 말씀을 전합니다. 또한, 학부생시절부터 항상 따뜻한 관심을 베풀어주신 조권회 교수님, 평소 아낌없는 격려와 도움을 주신 오철 교수님, 고민이 있을 때 마다 제 편에서 귀 기울여 들어주시고 조언을 해주시는 최재혁 교수님, 이원주 교수님께도 감사를 드립니다.

처음 대학원에 들어와 1년 동안 보조기계 연구실에서 석사생활에 적응하는데 도움을 주고 즐거운 추억들을 선물해준 황대중, 정창식, 황혜수 님께 감사드리며, 동기로서 항상 서로를 격려하고 응원해 주는 서범덕 학생에게도 감사를 전합니다. 또한, 찾아 갈 때마다 따듯하게 반겨주고 꼼꼼하지 못한 저를 세심하게 챙겨주는 학부사무실의 장아영, 이수빈, 박한경, 신경복 조교님들, 비록 동생이지만 형을 먼저 챙겨주고 힘든 일은 함께 고민해 주는 손광호, 못난 저를 친형

처럼 따르고 찾아와 주는 이동기, 그리고 도움이 필요할 때마다 흔쾌히 손을 내밀어 주신 레이저 연구실의 송무근 실장님께도 감사의 마음을 전하고자 합니다.

무엇보다 부족한 손자이자, 아들, 동생 그리고 오빠인 저를 항상 믿어주고 응원해주는 가족들에게 깊은 사랑을 전합니다. 이제 또 다른 시작이 기다리고 있기에 흥분도 되고 한편으로는 걱정도 앞서지만 가족들의 사랑과 믿음 속에서 슬기롭게 잘 헤쳐 나가도록 하겠습니다.

마지막으로 지면을 통해서 일일이 언급하지 못했지만 저를 아끼고 많은 관심을 베풀어 주신 모든 분들께 진심으로 감사의 말씀을 전합니다. 앞으로 더욱 열심히 그리고 성실하게 살아가도록 하겠습니다.

2019 기해년 사랑하는 모든 분들의 행복을 기원하며..